Martin Lasser, BSc.

Static gravity field determination from GOCE satellite data in a raw accelerometer data approach

MASTER'S THESIS

to achieve the university degree of

Diplom-Ingenieur

Master's degree programme: Geomatics Science

submitted to

Graz University of Technology

Supervisor

Univ.-Prof. Dr.-Ing. Torsten Mayer-Gürr

Institute of Geodesy
Working Group Theoretical Geodesy and Satellite Geodesy

Graz, September 2017

AFFIDAVIT

I declare that I have authored this thesis independently, that I have not used other than the declared sources/resources, and that I have explicitly indicated all material which has been quoted either literally or by content from the sources used. The text document uploaded to TUGRAZonline is identical to the present master‘s thesis.

14. September 2017

Date

Signature

Kurzfassung

Aufgrund der steigenden Anforderungen an die Schwerefeldbestimmung aus Satellitenmissionen, ist es notwendig neue Ansätze zur Auswertung der Daten zu verfolgen und zu verfeinern. Diese Arbeit stellt einen solchen vor, der die Möglichkeit bietet die rohen Akzelerometerdaten des GOCE EGG-Instrumentes zu verarbeiten, um ein statisches Schwerefeld daraus abzuleiten.
Im Gegensatz zum bisherigen Auswerteansatz der GOCE-Daten werden keine Linearkombinationen zwischen den Messungen einzelner Beschleunigungssensoren gebildet. Die Beobachtungen werden direkt mit den unbekannten Größen des Schwerefeldes sowie Störeinflüssen (Drift, Bias etc.) verknüpft. Dies führt für den Missionszeitraum von etwa vier Jahren mit sekündlicher Beobachtung von 22 Messgrößen zu einem sehr großen Gleichungssystem. Die Lösung wird über einen Ausgleich nach kleinsten Fehlerquadraten geschätzt.
Ziel ist es die Unsicherheiten in der Lösung des statischen Schwerefeldes zu reduzieren und eine einfachere Handhabung bezüglich aller Einflüsse zu bieten.

Abstract

Due to the increasing demand of extremely accurate gravity field determination other approaches than the ones specifically designed for a mission have to be investigated. This thesis depicts an approach of using the raw accelerometer data from GOCE EGG instrument to derive a static gravity field.
In contrast to the standard processing of GOCE accelerometer data it is designed considering the maxim not building any linear combinations as it is done when computing the common mode and differential mode accelerations. All unknown coefficients of the gravity field and other parameters, such as the sensor's bias and drift etc. that have to be determined to provide an accurate solution, were directly linked to the observations. As GOCE collected data over four years, measuring roughly every second, this leads to a large system of equations to be solved, with more than 500 Million observations. Since some quantities are of interest for the whole time span of measuring (e.g. gravity field coefficients) and some have to be calculated in every single epoch (e.g. common mode accelerations or the angular accelerations), more than hundred thousand unknown parameters occur. Solving is done in a least squares adjustment.
The goal of this approach is to reduce uncertainties in the static gravity field coinciding with the assumption of better error handling when using raw data.

Contents

Part I

Introduction

The demand of highly accurate static gravity field models is increasing, not only needs the task of creating a standardized and coherent height system for the globe a static gravity field in a tremendous precision but also a broad band of scientific communities is dependent from the accuracy of static gravity field solutions (e.g. the oceanography within ocean current models and the combination with alitmetry).
In 2009 the GOCE (Gravity field and steady-state Ocean Circulation Explorer) satellite mission from the European Space Agency (ESA) was launched. It was designed to measure the medium and short wavelength components of the gravity field to improve our knowledge about the system Earth together with its predecessor[1] GRACE (Gravity Recovery And Climate Experiment), which provides information about the long and medium wavelength components. The abbreviation GOCE shows the primary focus: A static gravity field for geophysical research on one hand and for oceanography on the other. The aim was creating a centimetre accurate geoid. Due to the focus on the higher degrees of the gravity field and its originally short mission period of less than two years, the main goal was the observation of the static components of the gravity field.
Achieving such a goal, it was necessary to measure the gravity field with an accuracy of less than 1 mgal ($= 10^{-5}\,\frac{\mathrm{m}}{\mathrm{s}^2}$) or spoken in terms of height with less than 1 cm in a spatial resolution of 100 km [Stummer (2006)]. This was succeeded in the normal processing. However, the processing of the core instrument, the EGG (Electrostatic Gravity Gradiometer), which is basically an array of six accelerometer within three orthogonal axes around the centre of mass of the satellite, leads to reconstructions of different necessary parameters (e.g. the angular rate reconstruction or the observations itself through the linear combination between certain axes) to determine the gravity field coefficients in a least squares adjustment (LSA). Consequently, this provides the possibility of uncertainties in the derived products.
In contrast, the raw accelerometer data approach (RADA) of processing discussed in this thesis tries to avoid all linear combinations or reconstructions by linking all unknown parameters (i.e. those of the gravity field and the perturbance variables, such as the common mode acceleration, drifts, biases etc.) directly to the observed accelerations. That implies 18 accelerometer measurements (one per axis, three axes per accelerometer, six accelerometers) and an attitude quaternion from the star camera, summing up to 22 observations per epoch and a large number of unknown parameters to determine, either per epoch or over the whole time span. For the GOCE mission's period this leads to 47 months of data with 22 observations roughly every second. Solving this in a least squares adjustment and deriving a gravity field, requires a careful consideration of the statement of the problem, demanding certain steps to be taken.
To describe those steps in detail the thesis is structured as follows:

Part II will give an overview about the GOCE mission, describing the satellite, the main goals and instruments, in particular the EGG instrument and its principles.

The following part III is dedicated to the mathematical background of gravity field modelling in case of gradiometry.

[1] In June 2017 after 14 years in orbit still working.

In part IV the measuring principle of satellite gravity gradiometry will be depicted and explained, including errors and the normal processing. This provides the fundamentals for part V where the raw accelerometer data approach is discussed in detail.

The results of the new approach are explained in part VI, together with a validation based on a comparison to other gravity field models.

To conclude the thesis, the last part gives an outlook with some notions on future improvements and prospective possibilities for the raw accelerometer data approach in GOCE data processing.

Part II

GOCE satellite mission

1 General overview

On the 17th of March 2009 the GOCE mission was launched with a delay of about two years from Plesetsk, Russia, as the first satellite of ESA's living planet programme, a programme which is dedicated to the observation of the planet Earth through various satellites (e.g. GOCE, CryoSat, Swarm etc.). The design life of GOCE was planned for 20 months with an observing phase of half a year. This was extended to four years and eight months in space, providing a bit less than four years of data. On 11th of November 2011 the mission came to an end with a spectacular picture of the vaporizing satellite during the re-entry in the Earth's atmosphere (see figure below).

Figure II.1: GOCE re-entry in Novmeber 2013[2]

The responsible mission control for GOCE was the ESOC (European Space Operations Centre) in Darmstadt, Germany, with data downlink stations in Kiruna (Sweden) and Svalbard (Norway). The instrument processing was done at ESA's Earth observation centre in Italy (European Space Research Institute - ESRIN); the evaluation of the data to derive gravity field products was handed over to several High-level Processing Facilities (HPF) in Europe under the leadership of the Technical University of Munich, a consortium consisting of research institutions as the Geoforschungszentrum in Potsdam (GFZ) and multiple universities, such as the Technical University of Graz and the University of Bern.
The satellite was built by 41 companies in 13 European countries, the leading ones being Thales Alenia Space in Italy and France, EADS Astrium GmbH in Germany and ONERA in France.

GOCE had a nearly polar, sun-synchronous orbit with an inclination of 96.7° and an orbital period of roughly 90 minutes in an altitude of around 250 km. In this constellation the orbit has a repeat cycle of

[2]Taken from http://www.esa.int/spaceinimages/Images/2013/11/ (June 2017)

61 days with a subcycle of 20 days. A global coverage is achieved after 30 to 40 days. Figure II.2 gives an overview of the GOCE orbit height and eclipse time during its lifetime.

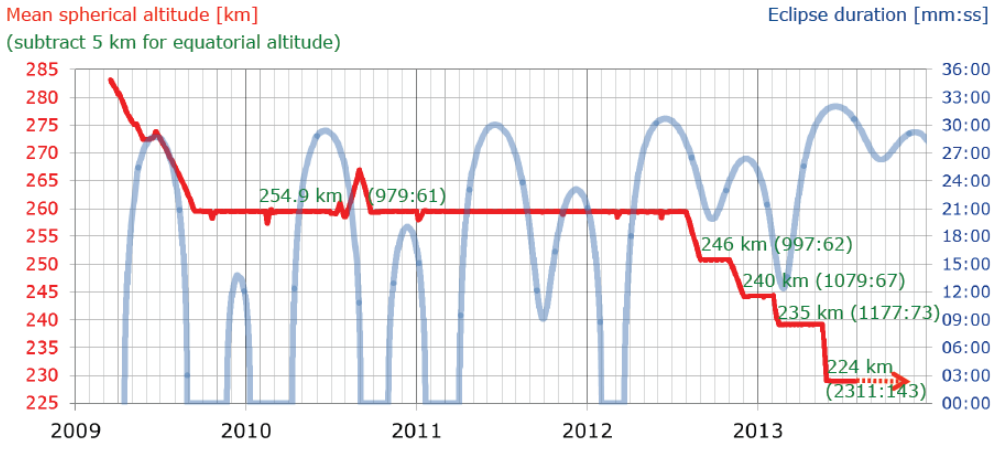

Figure II.2: GOCE: orbital height and eclipse time[3]

Due to the low altitude and the large atmospheric friction it was the first satellite to be built in aerodynamic shape (see figure II.3) with a mass of 1050 kg (including 205 kg payload mass), a size of 5.3 m in length and a body diameter of about 1 m. The atmospheric conditions in the very low orbit made it necessary to readjust the satellite's track continuously in order to prevent it from re-entering the Earth within days. To keep the satellite in its required position a drag compensation system with ion thrusters was mounted together with an attitude-control system.

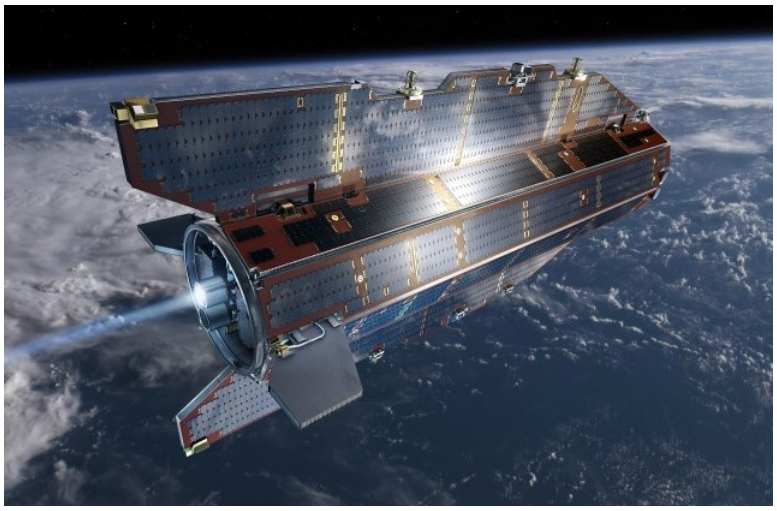

Figure II.3: The GOCE satellite[4]

Well summarized information on the satellite, the mission and the orbit can be found at:
http://www.esa.int/Our_Activities/Observing_the_Earth/GOCE/Facts_and_figures (June 2017)
and as well at the Earth Observation Portal (eoPortal), operated by the European Space Agency [ESA (2017)].

[3]Source: Gruber, T. and Rummel, R. (2014)
[4]Taken from: https://earth.esa.int/web/sppa/mission-performance/esa-missions/goce; ESA-AOES-Medialab (June 2017)

GOCE had three major instruments. Its primary instrument, the EGG, was a complete new development and the first time that gradiometry was used in space. The other instruments included a dual frequency GPS (Global Positioning System) receiver for Satellite-to-Satellite Tracking - High-Low (SST-hl) and the Advanced Drag Compensation and Attitude Control System (DFACS - Drag-Free Attitude Control System), to keep the satellite in orbit and the accelerometers near free fall motion. Furthermore, a retro reflector for Satellite Laser Ranging was affixed.
The mission costs occasioned by about 350 Million Euro.
A summary of the most important facts is given in table II.1 below.

Table II.1: fact sheet GOCE

name	GOCE
operator	ESA
mass	1050 kg including 40 kg of xenon
size	5.3 m length × 1 m (body diameter)
orbit	sun-synchronous, 61days repeat
altitude	250 km
inclination	96.7°
eccentricity	0.000932
orbital period	89.3 min
mission start	March, 17th, 2009
mission end	November 11th, 2013
costs	350 Mio. Euro

2 Instruments

For any evaluation of data the understanding of the instruments and their working principles form the basis of all further development. GOCE had two main instruments to measure quantities of the gravity field. The core of the mission, the gradiometer (EGG), which was the first time that the principle of Satellite Gravity Gradiometry (SGG) was applied, and the GPS receiver for Satellite-to-Satellite-Tracking. Moreover, some instruments to provide the fundamentals for the two above mentioned were mounted. All of them interact and cannot be considered completely independent from each other. This chapter gives a short description of the instruments, how they concur and their role in the data analysis process. Well summarized information on the instruments can be found in the short paper GOCE and its Gravity Measurement Systems [Fehringer et al. (2008)] and the eoPortal for the GOCE satellite [ESA (2017)] .

GPS receiver (SST-hl)

Since the gradiometer can only detect the medium and short wavelength components of the gravity field due to its measuring bandwidth and the accurate position of any measurement is necessary for further analysis, a GPS receiver was fitted to the GOCE satellite. It provided the locating of the gradiometer observations and the utilisation of Satellite-to-Satellite-Tracking high-low technique to derive the long and medium wavelength components of the gravity field from a precise satellite orbit. In SST-hl the orbit is determined through observations from the low orbiting satellite (GOCE) to higher navigation satellites (GPS in this case). Because the signal of the gravity field decreases quadratic with the distance from the source, a lower orbit is more suitable for the determination of the shorter wavelengths of the gravity field. However, the

lower the orbit, the more drag from the atmosphere interacts with the satellite and it becomes necessary to separate the friction signal from the gravity signal through independent observations. Considering that, the EGG instrument data is used in the SST-hl technique. Figure II.4 gives an overview of the SST-hl principle

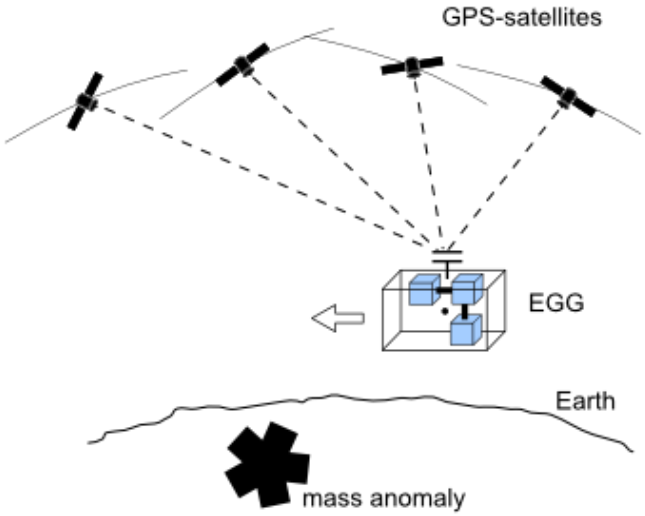

Figure II.4: SST-hl with GOCE[5]

The orbit of a satellite is directly related to the gravity field, therefore, the latter can be ascertained through the satellite's track. Since the accuracy of orbit determination is limited to a certain extant, only the long wave components up to degree 60 can be derived from the SST-hl for GOCE [ESA (2006)]. As the gradiometer resolution starts at around degree 15, an overlap of about 45 degrees can be obtained. Within more recent models the SST-hl solution reaches up to degree and order 150, see Brockmann et al. (2014)
The GOCE receiver could observe (cf. ESA (2006))

- 6 carrier phase measurements from 6 GPS satellites at the frequency of L1,
- 6 carrier phase measurements from 6 GPS satellites at the frequency of L2,
- 6 C/A-code pseudo-range measurements from 6 GPS satellites at L1 and
- 6 P-code pseudo-range measurements from 6 GPS satellites at L1, as well as
- 6 P-code pseudo-range measurements from 6 GPS satellites at L2.

Gradiometer (EGG)

The Electrostatic Gravity Gradiometer was the core instrument and heart of GOCE. It had a measuring bandwidth between 5 mHz and 100 mHz [Stummer (2006)], which maps a spatial resolution between 80 km and 1500 km or respectively a spherical harmonic degree of 13 to 250. As already mentioned, it was composed of six capacitive accelerometers. They were produced by the French company ONERA.
In general an accelerometer is made of a casing and a proof mass, which can move relative to the casing.

[5] cf. ESA (2006)

When the accelerometer is accelerated, the proof mass follows the inertia force and moves relative to to the casing. The length of the displacement is measured to obtain the acceleration. An accelerometer in rest at the Earth's surface observes around 9.8 m/s^2, in free fall 0 m/s^2. Since the seismic mass and the casing in free fall move at the same speed, there is no relative displacement. There are two types of accelerometers: Instruments, in which the displacement itself is taken into account to derive acceleration and instruments, in which a force is applied to keep the seismic mass balanced at the same position at all time. The quantity of the applied force, mostly voltage, is measured and converted into acceleration. In case of GOCE the latter type was used.
All six accelerometers of GOCE had the same structure. They were three dimensional with orthogonal axes. A servo-driven electrostatic suspension with six degrees of freedom controlled the proof mass, which was floating in a small cage, towards translation and rotation. The precision was $6 \cdot 10^{-8}\,\mathrm{m}/\sqrt{\mathrm{Hz}}$ for the translation and 10^{-3} rad for the rotation [ESA (2006)]. Two plates of electrodes and a ring plate encased the proof mass and formed a capacitive sensor (see figure II.5).

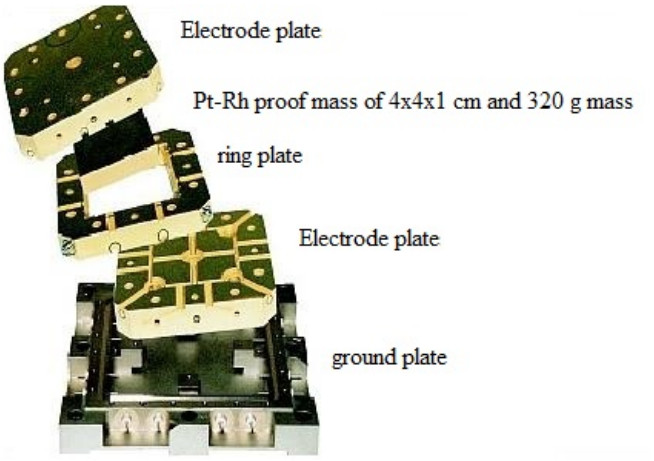

Figure II.5: Structure of a GOCE accelerometer[6]

A movement of the seismic mass caused an immediate variation in the capacity, which was readjusted. The force needed to readjust was measured and converted into acceleration. The conversion was assumed to be closely linear and the threshold for a quadratic factor was set to 1 s^2/m/month. As Berge et al. (2011) state, this was achieved and surpassed by the factor 10 in the first two years of measuring, however, as investigations showed, later the threshold was exceeded. In the new approach of this thesis this impact is included.
The proof mass had a size of 4x4x1 cm, was made of paltinium-rhodium alloy, weighting 320 grams. One edge was four times shorter than the others because in necessary ground tests one axis is always subjected to Earth's gravity. Hence, every accelerometer consisted of two ultra sensitive axes with a precision of $2 \cdot 10^{-12}\,\frac{\mathrm{m}}{\mathrm{s}^2}/\sqrt{\mathrm{Hz}}$ and one less sensitive axis with $1 \cdot 10^{-10}\,\frac{\mathrm{m}}{\mathrm{s}^2}/\sqrt{\mathrm{Hz}}$ [Stummer (2006)]. This leads to a special arrangement within the gradiometer.
The six accelerometers were arranged in pairs on three axes around the centre of mass (CoM) of the satellite, fixed on an ultra stable carbon-carbon honeycomb support structure [Fehringer et al. (2008)]. This is depicted in figure II.6. Note that the less precise shorter edges point into y- and z-direction, but not along track into x.

[6] Taken from eoPortal: https://directory.eoportal.org/web/eoportal/satellite-missions/g/goce (June 2017)

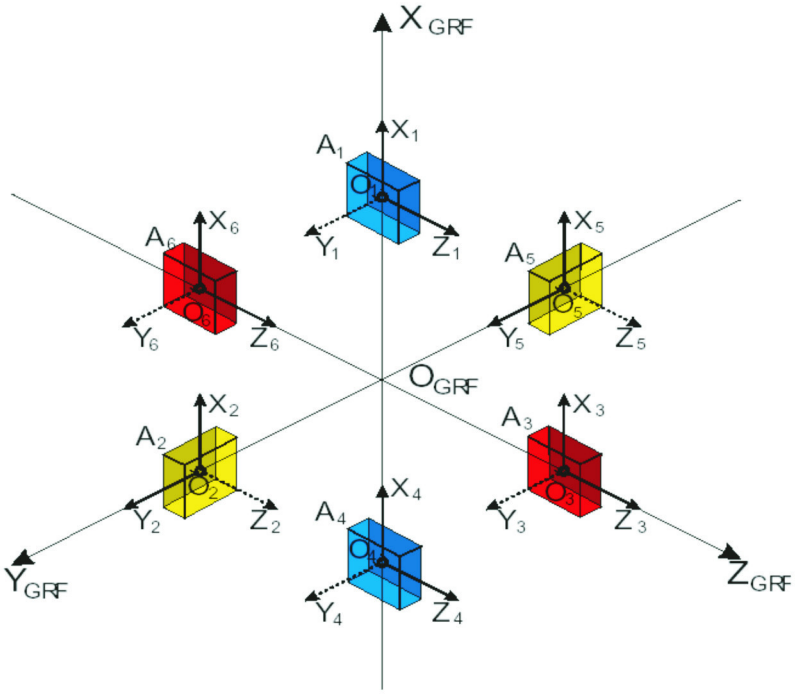

Figure II.6: Arrangement of the accelerometers in the Gradiometer[7]

The axes were, by definition, strictly orthogonal and each accelerometer was affixed in a distance of 25 cm to the CoM. Consequently, the baseline on one axis is 50 cm long. The two accelerometers along one baseline form one arm of the gradiometer. The whole instrument as well as one arm are shown in figure II.7.

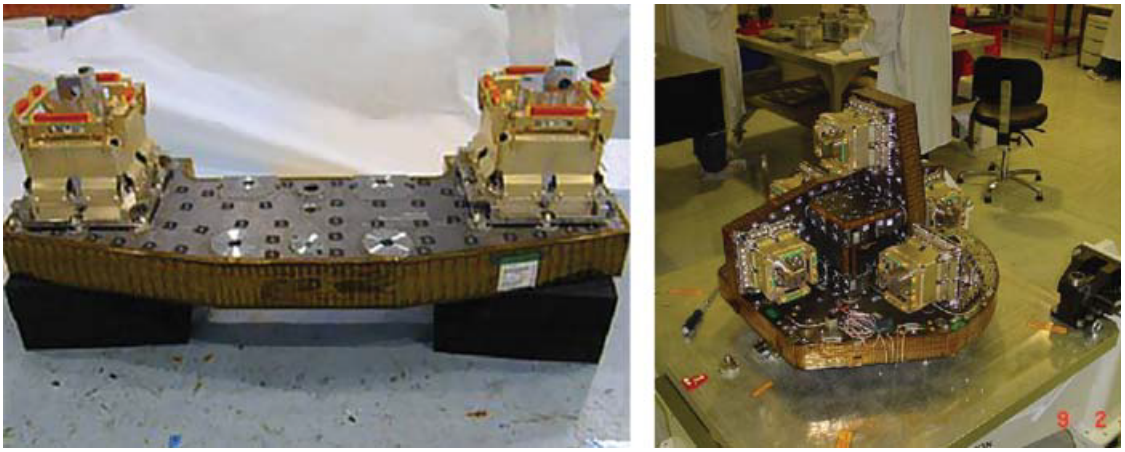

Figure II.7: Gradiometer arm (left) and the whole EGG (right)[8]

The arms consisted of the pairs A1-A4 (blue in figure II.6), as well as A2-A5 (yellow) and A3-A6 (red). All three arms of the EGG have their origin, by definition, in the CoM. These three baselines build the Gradiometer Reference Frame (GRF), where the gradiometer measurements took place (see part IV). The x-axis showed approximately in flight direction (along-track), the y-axis across-track and the z-axis radially

[7] Taken from GOCE Level 1b Products User Handbook (2006)
[8] Taken from GOCE and its Gravity Measurment Systems, Fehringer et al. (2008)

outwards, forming a right-handed coordinate system. The arrangement, which axes in the GRF were formed by the sensitive axes and which by the less sensitive axes of the accelerometers was chosen to provide best measurements for the main diagonal elements of the gravity tensor V_{xx}, V_{yy}, V_{zz} and for the angular velocity ω_y perpendicular to the along track, as this angle goes from $0°...360°$ within one revolution [Stummer (2006)]. Likewise, the crucial determination of the atmospheric drag for the drag compensation was taken into account in the arrangement of the accelerometers, manifesting in the fact that only high sensitive axes pointed in flight direction.
For each accelerometer the ARF (Accelerometer Reference Frame) exists, which has its origin in the centre of the accelerometer and the axes are parallel to the axes of the GRF.

Star camera

In GOCE three star cameras (also referred to as star trackers or star sensors) were integrated, based on the developments of star trackers made with CHAMP[9] and GRACE. They were mounted as close as possible to the EGG, such that none of them is dazzled by the sun or Earth and maximum one is blinded by the moon. At least the data of two was transmitted to Earth [Siemes (2011)].
In general a star tracker takes a picture from the starry sky and detects stars using image processing. After some corrections, the detected stars are matched to a star catalogue, from which the current attitude of the satellite can be derived. The star cameras provided a solution for the current attitude better than three arc seconds in spatial directions and better than 24 as in line of sight [ESA (2017)]. The control system decided, which of the three cameras was used. Attitude data from the star trackers was not only incorporated in the attitude control but also in the computation of the angular rates in the angular rate reconstruction (see part IV - HPF approach), where the exact angular rates in all frequencies are sought-after and the EGG alone does not provide enough information, especially in the low frequencies. The star camera system of GOCE can be seen in figure II.8. Note the small size of a star tracking device.

Figure II.8: Star tracker device, note the coin as a size comparison[10]

[9] Challenging Minisatellite Payload, satellite from the GFZ, launched 2000
[10] Taken from the eoPortal: https://directory.eoportal.org/web/eoportal/satellite-missions/g/goce (June 2017)

Drag-free and attitude control system

The DFACS had the task to maintain the satellite's attitude and keeping the satellite in a drag-free state of free fall, where only the conservative forces act. Therefore, ideally the friction acceleration is not measured with the accelerometers in the EGG. It received the necessary data from the gradiometer, the star cameras and three magnetometers as well as the Earth- and the sun-sensor to monitor and readjust the attitude of the satellite, preventing it from lurching and balancing it in a drag-free state. For any manoeuvres that keep the drag-free state the common mode accelerations were used to compensate the friction through an on-board ion propulsion assembly with a supply of 41 kg xenon and 0.6 to 20 mN thrust. Furthermore, a cold gas propulsion system running on nitrogen with 13.1 kg propellant and 0.6 mN thrust was mounted for the satellite shaking in the calibration phases. In addition three magnetotorquers were in use to maintain the attitude.

Other subsystems

For the sake of completeness the other subsystems of GOCE are mentioned here, cf. ESA (2017).

Avionics and Radio Frequency Subsystem (RFS) The RFS was responsible for the up- and downlink of data. Communication was done using two coherent S-band transponders, two hemispherical antennas on solar array edges and a radio frequency distribution unit with an uplink data rate of 4 kbit/s and a downlink data rate up to 1.2 Mbit/s. Communication stations were in Norway (Svalbard) and Sweden (Kiruna) catching the satellite on its nearly polar orbit as often as possible. However, typically one link lasted five minutes, resulting in an average of 26 minutes of communication per day. The satellite was able to autonomously operate for 72 hours without loss of science data.

Control unit and data handling system It was an on-board control unit that provided essential computational power for the control of the systems on-board, including a four Gigabyte mass storage for scientific data.

Power supply system The power supply system worked with fixed gallium-arsenide (GaAs) cell solar panels, which had a power of 1.3 kW and Li-ion batteries, made of 52 strings with 8 cells each with a battery storage capacity of 78 Ah. Due to the sun-synchronous orbit the maximum eclipse time was about 30 minutes.

Thermal control For the thermal control the EGG instrument was fully thermally decoupled from the satellite. Besides the passive thermal control, all heaters were software controlled.

3 Data

For any evaluation certain data products are available, depending which target is pursued. Usually the raw data, which is downlinked from the satellite, contains science and housekeeping data and remains in the hands of the operator. It is not published. The following description is based on the GOCE Level 1b Products User Handbook, ESA (2006).
In the first processing steps of the raw downlinked data a time tagging is added. Satellite and instrument housekeeping data (including the attitude) is given at 2 Hz, the output of the six accelerometers is given at 1/0.999360 Hz and the SST data at 1 Hz (Level 0 products).

The least preprocessed data released is Level 1b data. The processing of Level 1b data from Level 0 data is carried out by the instrument processing facility (ESRIN, Italy). In this step the conversion into engineering units (e.g. voltages into m/s^2), corrections, calibrations, a simple outlier detection and geolocation of the data along the orbit are done. Also the first steps of processing, i.e. the angular rate reconstruction and the linear combinations for the gravity gradients are part of the computation of Level 1b data.
Level 1b data includes

- EGG and star camera data,
- attitude (from the star trackers) and orbit data (position, velocity and time),
- gravity gradients in GRF and the rotation GRF to Inertial Reference Frame (IRF),
- frame transformation matrices,
- common mode accelerations, angular rates and angular accelerations,
- SST measurements and derived positions and reconstructed satellite orbits in Earth-Fixed Reference Frame (EFRF).

Level 2 products are any products derived from the latter level, such as gravity field models, precise orbits etc.

In this thesis the calculation of such a Level 2 product, a static gravity field, from Level 1b data is accomplished. For the raw accelerometer data approach solution the whole available Level 1b data of the EGG instrument was used. The data set consists of 47 months of almost 1 Hz sampling of accelerometer and star tracker data, summing up to more than two billion observations without the orbit data.
To located the measurements, a Reduced Dynamic Orbit, i.e. an orbit based on observations and physical models, was derived from the GPS data. As this amount of data is too large for an efficient gravity field determination, the observations were filtered and then down sampled to 5 seconds, leaving around 500 million data points.

Part III

Theoretical background

To give a short introduction in the mathematics of gravity field modelling and the raw accelerometer data approach, this chapter summarizes some physical and mathematical background.

Newton's law of gravitation reads as follows

$$\mathbf{F}_{12} = \frac{Gm_1m_2}{l^2}\mathbf{e}_{12}, \tag{III.1}$$

providing information about the force acting between the mass m_1 and the mass m_2 in a distance l with the unit vector $\mathbf{e}_{12}$ between m_1 and m_2 and the universal gravitational constant G.
The force field build up by gravitation is conservative[11] and therefore a potential function exists. The potential of the Earth as a homogeneous sphere can be written as

$$V = \frac{GM}{R}, \tag{III.2}$$

with GM as the product of the universal gravitational constant and the mass of the Earth and R as the Earth's radius. Considering the oblateness of the Earth and other inhomogeneities, a natural way to express the potential is the expansion in any series. In case of the gravity field outside the Earth, a series fulfilling the Laplace equation

$$\Delta V = V_{xx} + V_{yy} + V_{zz} = 0 \tag{III.3}$$

makes sense, since there are no external sources of gravity. Following the rule that every series consists of basic functions and coefficients, the potential may be written as

$$V = \frac{GM}{R}\sum_{n=0}^{N}\left(\frac{R}{r}\right)^{n+1}\sum_{m=0}^{n}\left[c_{nm}\cos(m\lambda) + s_{nm}\sin(m\lambda)\right]P_{nm}(\cos\vartheta), \tag{III.4}$$

with the coefficients c_{snm} and s_{nm}. The Legendre functions P_{nm}, i.e. the m^{th}derivation of the Legendre polynomial P_n and the $\cos(m\lambda)$ and $\sin(m\lambda)$ terms form the spherical harmonics, which fulfil the condition given in equation III.3. The point of calculating the potential is given by the radius r, the pole distance ϑ and the geographical longitude λ. R defines the radius of the Earth, for calculations on the surface in spherical approximation $r = R$ is valid.
Despite the already explained parts, the coefficients have to be known. In theory the series is infinite, still it has to be truncated for practical applications at any point. Recent global satellite data based models go up to degree n and order m 280 as the last GOCO05s model, computed by Mayer-Gürr et al. (2015) or the latest GOCE-time-wise-approach release TIM5, Brockmann et al. (2014). This represents a spatial resolution of a bit more than 70 km on the Earth's surface.
In case of this thesis the coefficients are the parameters sought-after. Still, it is necessary to find a relation between the measured accelerations in the EGG and the potential.

[11] Easiest proof: The field is curl-free $\nabla\times\mathbf{F} = 0$

If the second derivation of the potential is built in all directions, a tensor matrix is reached, containing

$$\mathbf{T} = \nabla\nabla V = \begin{bmatrix} V_{xx} & V_{xy} & V_{xz} \\ V_{yx} & V_{yy} & V_{yz} \\ V_{yz} & V_{zy} & V_{zz} \end{bmatrix}, \tag{III.5}$$

with the trace being zero (equation III.3) and a symmetric behaviour. Hence, only five components are independent.
The spherical harmonics expansion in radial direction, which is easier to build in spherical coordinates, may be written as

$$V_{rr} = \frac{GM}{R} \sum_{n=0}^{N} \left(\frac{R}{r}\right)^{n+1} \frac{(n+1)\cdot(n+1)}{R} \sum_{m=0}^{n} \left[c_{nm}\cos(m\lambda) + s_{nm}\sin(m\lambda)\right] P_{nm}(\cos\vartheta) \tag{III.6}$$

Considering the unit of the tensor, the second derivation cancels out the length component and leaves $[1/\mathrm{s}^2]$. Thus, it is easy to find a connection between accelerations when measured along a known distance as given by the EGG's baselines and the coefficients of such a spherical harmonics expansion. As the gradient in gravity field modelling gets small, the unit Eötvös [E], named after the Hungarian physicist Loránd Eötvös, is introduced with $1\mathrm{E} = \frac{1}{\mathrm{s}^2} \cdot 10^{-9}$.

Part IV

Measuring principle of Satellite Gravity Gradiometry

The Satellite Gravity Gradiometry is based on the assumption, that the CoM of the satellite remains in the state of free fall when orbiting around Earth. Without any friction an accelerometer in the CoM measures zero acceleration because the proof mass and the casing are falling at the same speed. In satellite gradiometry the six accelerometers of the EGG are placed on three orthogonal axes in a known distance from the CoM. The reference frame (GRF), which is defined by the three axes of the gradiometer, is formed with the first axis in flight direction, the third axis pointing radially outwards and the second axis pointing roughly across-track building an orthogonal triad (see figure IV.1).

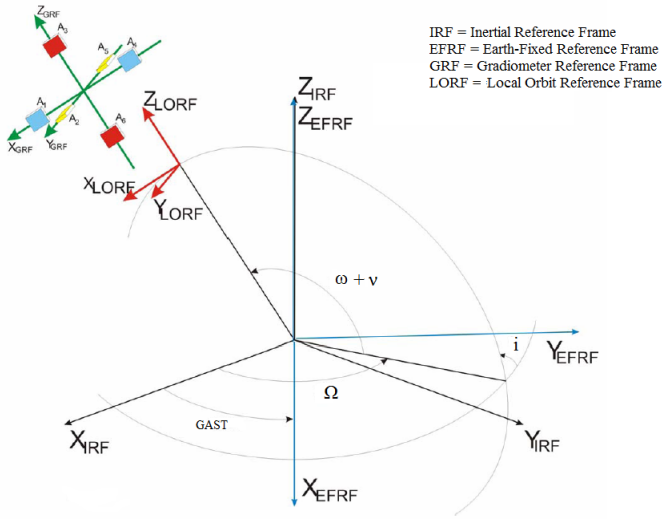

Figure IV.1: Most important GOCE reference frames[12]

All measurements of the EGG are referred to the GRF, however each accelerometer has its own reference frame (ARF). Still, nominally the axes of the ARFs are parallel to the GRF. Hence, the measurements can be considered as being observed in the GRF.
As the accelerometers do not coincide with the CoM, every accelerometer measures an acceleration. A short gedankenexperiment shall underline which acceleration is observed:
Keeping the satellite at a constant position and considering only the axes pointing radially from the Earth (Z_{GRF}, see figure IV.1), the accelerometers as well as the satellite are attracted by the Earth, with A6 being more attracted as it is closer to the source and the attraction acceleration decreasing with $\frac{1}{l^2}$ (see equation III.1). The second in size of acceleration towards the Earth is the CoM, and lastly the accelerometer A3. This leads to a displacement in the accelerometers similar to high-tide. Therefore, the measured acceleration can be explained by tidal accelerations depending on the tidal potential and the distance to the common mass centre between the Earth and the satellite. As the tides are only caused by the Earth's gravity field, the tidal tensor can be described with Earth's gravity tensor. Being in the GRF the common centre of mass

[12]Source: GOCE Level 1b Products User Handbook (2006)

between the Earth and the satellite is exactly the CoM. Thus, the measured acceleration for an accelerometer is

$$\mathbf{a} = -\mathbf{T} \cdot \mathbf{r},$$

with $\mathbf{T}$ as the tensor from equation III.5 and $\mathbf{r}$ the position vector of the accelerometer, i.e. the distance to the CoM. The sign before the tensor comes from the measuring principle. Since closed loop accelerometers are mounted, not the displacement itself is measured but the force needed to keep the proof mass in balance. This force acts in the opposite direction as the displacement (Newton's third law).
In contrast to our gedankenexperiment the satellite is orbiting around Earth. Thus, it is in constant rotation and apparent forces are observed in the GRF as well. Those are the centrifugal force because of the angular rate of the rotation (ω) and the Euler force due to the change of the rotation axis ($\dot{\omega}$). The apparent forces depend on the distance $\mathbf{r}$. There is no Coriolis force, since the accelerometers cannot move in the GRF.
Hence, the observation equation may be written as

$$\mathbf{a} = -\mathbf{T} \cdot \mathbf{r} + \omega \times (\omega \times \mathbf{r}) + \dot{\omega} \times \mathbf{r} \tag{IV.1}$$

with the measured acceleration $\mathbf{a}$, which is now divided into three parts. The first part on the right hand side $-\mathbf{T} \cdot \mathbf{r}$ represents the amount of acceleration generated by the gravitational potential. The second component $\omega \times (\omega \times \mathbf{r})$ is the measured centrifugal force caused by the mounting offset of the accelerometer to the CoM and the resulting angular rates. $\dot{\omega} \times \mathbf{r}$ is the acceleration of the proof mass due to the angular acceleration.
Writing out the components in full gives

$$\mathbf{T} = \begin{bmatrix} V_{xx} & V_{xy} & V_{xz} \\ V_{yx} & V_{yy} & V_{yz} \\ V_{yz} & V_{zy} & V_{zz} \end{bmatrix}, \quad \mathbf{r} = \begin{bmatrix} r_x \\ r_y \\ r_z \end{bmatrix}, \quad \omega = \begin{bmatrix} \omega_x \\ \omega_y \\ \omega_z \end{bmatrix} \text{ and } \dot{\omega} = \begin{bmatrix} \dot{\omega}_x \\ \dot{\omega}_y \\ \dot{\omega}_z \end{bmatrix}. \tag{IV.2}$$

Computing the cross products in equation IV.1 and a short rearranging leads to a separation in the tensor itself, a symmetric part and a skew-symmetric component

$$\begin{bmatrix} a_x \\ a_y \\ a_z \end{bmatrix} = \left(- \begin{bmatrix} V_{xx} & V_{xy} & V_{xz} \\ V_{yx} & V_{yy} & V_{yz} \\ V_{zx} & V_{zy} & V_{zz} \end{bmatrix} + \begin{bmatrix} -\omega_y^2 - \omega_z^2 & \omega_x\omega_y & \omega_x\omega_z \\ \omega_x\omega_y & -\omega_x^2 - \omega_z^2 & \omega_y\omega_z \\ \omega_x\omega_z & \omega_y\omega_z & -\omega_x^2 - \omega_y^2 \end{bmatrix} + \begin{bmatrix} 0 & -\dot{\omega}_z & \dot{\omega}_y \\ \dot{\omega}_z & 0 & -\dot{\omega}_x \\ -\dot{\omega}_y & \dot{\omega}_x & 0 \end{bmatrix} \right) \begin{bmatrix} r_x \\ r_y \\ r_z \end{bmatrix}, \tag{IV.3}$$

or in matrix-vector notation

$$\mathbf{a} = (-\mathbf{T} + \mathbf{\Omega\Omega} + \dot{\mathbf{\Omega}})\mathbf{r} \tag{IV.4}$$

This is the observation equation of Satellite Gravity Gradiometry. However, equation IV.3 is only valid in a system without external influences. Only rotations and the conservative force (i.e. the gravity field) are considered in this equation. As shown later, the non-conservative forces acting on the satellite have to be included as well.
Another approach of explaining Satellite Gravity Gradiometry is given in Stummer (2006).

1 Errors

So far the described observation equation is based on the assumption of an ideal gradiometer. However, in reality the accelerometers show a lot of different error behaviours. On one hand there are random errors due to the measurement noise and on the other hand systematic errors appear, i.e. bias, scaling (linear, quadratic), misalignment of the axes (they do not for a parallel system w.r.t. the GRF) and non-orthogonality of the accelerometer axes (the axes of the ARF do not form a strictly orthogonal triad). These systematic errors are instrument errors, which can be found on every single accelerometer. Also, the gradiometer arm lengths can vary or at least differ from the nominal length and finally the conversion from voltages to engineering units may underlie a drift.
For a detailed summary of the errors in SGG see Stummer (2006).

Random errors

Within every measurement system errors occur due to the imperfections of the system itself. They manifest as noise. Unlike systematic errors they act randomly in all directions, following a Gaussian distribution. As mentioned before, the accelerometers measure with a precision of $2 \cdot 10^{-12} \frac{\mathrm{m}}{\mathrm{s}^2}/\sqrt{\mathrm{Hz}}$ in the high sensitive axes and $1 \cdot 10^{-10} \frac{\mathrm{m}}{\mathrm{s}^2}/\sqrt{\mathrm{Hz}}$ in the less sensitive axis in a measuring bandwidth of 5 mHz to 100 mHz. Outside the measuring bandwidth these values are not representative. The star camera's standard deviation lies between 3 and 24 arc seconds.
The random errors have to be considered carefully in the computation of the gravity field, especially when it comes to the validation of the quality of the derived product.

Bias

The bias is an error occurring at each accelerometer individually. It is an offset from the nominal measurement and distorts all observations systematically. It can be found in all axes and over all frequencies. Thus, there are 18 unknown bias-quantities. The bias does not remain constant over time and therefore, it has to be determined frequently. Written as equation for one accelerometer, the bias $\mathbf{b}$ occurs as a constant

$$\mathbf{a}_{measured} = \mathbf{a}_{true} + \mathbf{b}, \tag{IV.5}$$

where $\mathbf{a}_{true}$ corresponds with the acceleration in equation IV.4.

Scale factor

Similar to the bias, the scale factor is an error that affects all accelerometers and axes. Basically, it is the multiplication of the true acceleration with a constant value, thus appearing in all frequencies. The scale factor may be explained with "[...] uncertain knowledge of the electrostatic gains and the read-out gain for the conversion of the electrode control voltages to accelerations" [Siemes (2011)]. Without other influences, it may be written as

$$\mathbf{a}_{measured} = \mathbf{S} \cdot \mathbf{a}_{true}, \tag{IV.6}$$

where $\mathbf{S}$ is a diagonal matrix containing the scaling factors s_x, s_y, s_z.

$$\mathbf{S} = \begin{bmatrix} s_x & 0 & 0 \\ 0 & s_y & 0 \\ 0 & 0 & s_z \end{bmatrix}. \tag{IV.7}$$

The scaling does not have to remain constant over time; a potential trend leads to

$$\mathbf{S} = \begin{bmatrix} s_{0,x} + s_1(t - t_0) & 0 & 0 \\ 0 & s_{0,y} + s_{1,y}(t - t_0) & 0 \\ 0 & 0 & s_{0,z} + s_{1,z}(t - t_0) \end{bmatrix} \tag{IV.8}$$

with t denoting the current epoch and t_0 the reference epoch (e.g. t_0 is the first epoch of a month for monthly estimation of the scale factors).
Factoring out the identity matrix $\mathbf{I}$ of the scale matrix $\mathbf{S}$

$$\mathbf{S} = (\mathbf{I} + \mathbf{\Delta S}) \tag{IV.9}$$

the error can be obtained via

$$\mathbf{a}_{measured} = (\mathbf{I} + \mathbf{\Delta S})\, \mathbf{a}_{true} = \mathbf{a}_{true} + \Delta\mathbf{S} \cdot \mathbf{a}_{true} \tag{IV.10}$$

with $\Delta\mathbf{S} \cdot \mathbf{a}_{true}$ denoting the influence of the scaling.

Non-orthogonality of the accelerometer axes

If the axes within an accelerometer are not strictly orthogonal, the signal from one axis is projected into another. Thus, the observations include the true signal and the coupling between the axes. Hence, the measured acceleration may be considered as a shear of the true acceleration

$$\mathbf{a}_{measured} = \mathbf{E} \cdot \mathbf{a}_{true} \tag{IV.11}$$

with the shear matrix $\mathbf{E}$. Since the shear can be assumed to be small, it may be written as

$$\mathbf{a}_{measured} = (\mathbf{I} + \Delta\mathbf{E})\, \mathbf{a}_{true}, \quad \mathbf{a}_{measured} = (\mathbf{I} + \begin{bmatrix} 0 & \alpha & \beta \\ \alpha & 0 & \gamma \\ \beta & \gamma & 0 \end{bmatrix})\, \mathbf{a}_{true}, \tag{IV.12}$$

where the error component $\Delta\mathbf{E} \cdot \mathbf{a}_{true}$ contains the infinitesimal shear angles γ (x-axis), β (y-axis) and α (z-axis).

Misalignment

The misalignment refers to a wrong orientation of the ARF with respect to the GRF. If the axes of the ARF are not strictly parallel to the ones in the GRF, the signal between two axes cannot be separated correctly. Therefore, it may be described as a rotation between the ARF and the GRF. Assuming infinitesimal small rotation angles given in δ, ε and ζ (x,y,z-axis respectively) the measured and the true accelerations are

connected with

$$\mathbf{a}_{measured} = (\mathbf{I} + \begin{bmatrix} 0 & \zeta & -\varepsilon \\ -\zeta & 0 & \delta \\ \varepsilon & -\delta & 0 \end{bmatrix}) \, \mathbf{a}_{true}. \tag{IV.13}$$

The rotation matrix is defined as

$$\mathbf{R} = \mathbf{I} + \Delta\mathbf{R} = \mathbf{I} + \begin{bmatrix} 0 & \zeta & -\varepsilon \\ -\zeta & 0 & \delta \\ \varepsilon & -\delta & 0 \end{bmatrix}. \tag{IV.14}$$

The magnitude and the impact of the last two errors are similar, see Stummer (2006).

Offset of a gradiometer arm

Even if there are no instrument errors, the whole system working in SGG is disturbed when the origin of the axes of the gradiometer does not coincide with the CoM. The whole background given in part IV is only valid under the assumption that the gradiometer's origin coincides with in the CoM. If not, the offset has to be corrected. This means that the distance of each accelerometer to the centre of mass (roughly 25 cm) has to be adjusted. The offset has three components o_x, o_y and o_z. The correction of the accelerometer positions is given in the following overview, cf. Stummer (2006).

$$\begin{aligned}
A_1 : \begin{bmatrix} r_x \\ r_y \\ r_z \end{bmatrix} &= \begin{bmatrix} \frac{L_x}{2} + o_x \\ +o_y \\ +o_z \end{bmatrix}; \quad A_4 : \begin{bmatrix} r_x \\ r_y \\ r_z \end{bmatrix} = \begin{bmatrix} \frac{-L_x}{2} + o_x \\ +o_y \\ +o_z \end{bmatrix}; \\
A_2 : \begin{bmatrix} r_x \\ r_y \\ r_z \end{bmatrix} &= \begin{bmatrix} +o_x \\ \frac{L_y}{2} + o_y \\ +o_z \end{bmatrix}; \quad A_5 : \begin{bmatrix} r_x \\ r_y \\ r_z \end{bmatrix} = \begin{bmatrix} +o_x \\ \frac{-L_y}{2} + o_y \\ +o_z \end{bmatrix}; \\
A_3 : \begin{bmatrix} r_x \\ r_y \\ r_z \end{bmatrix} &= \begin{bmatrix} +o_x \\ +o_y \\ \frac{L_z}{2} + o_z \end{bmatrix}; \quad A_6 : \begin{bmatrix} r_x \\ r_y \\ r_z \end{bmatrix} = \begin{bmatrix} +o_x \\ +o_y \\ \frac{-L_z}{2} + o_z \end{bmatrix}.
\end{aligned} \tag{IV.15}$$

Thus, the accelerometer positions referring to the true CoM consist of the gradiometer arm lengths L and the offset o. According to Stummer (2006) the offset is at most 2 cm.

Non-linear conversion from voltages

The conversion from measured voltages to engineering units in accelerometers shall be closely linear. However, it is known that the behaviour of the instruments may vary over time and the conversion underlies a drift. This problem can be solved within the accelerometer's hardware through voltage corrections. Otherwise, it can be described approximately by a quadratic term. The observation equation including the quadratic factor k_2 may be written as

$$\mathbf{a} = (-\mathbf{T} + \boldsymbol{\Omega}\boldsymbol{\Omega} + \dot{\boldsymbol{\Omega}})\mathbf{r} + k_2[(-\mathbf{T} + \boldsymbol{\Omega}\boldsymbol{\Omega} + \dot{\boldsymbol{\Omega}})\mathbf{r}]^2. \tag{IV.16}$$

As one can see, the unit of the quadratic factor is [s²/m/month]. Investigations for data from 2009 to 2011 showed that the quadratic factor did not exceed the 0.11 s²/m/month, which is nine times better than

the requirement [Berge et al. (2011)]. However, according to investigations for this thesis and also to an information from C. Siemes it was exceeded from 2011 onwards.

2 Observation equation of SGG

Summing up all errors that occur within one accelerometer the observation equation may be written as

$$\mathbf{a}_{measured} = \mathbf{a}_{true} + \mathbf{b} + \Delta\mathbf{S} \cdot \mathbf{a}_{true} + \Delta\mathbf{E} \cdot \mathbf{a}_{true} + \Delta\mathbf{R} \cdot \mathbf{a}_{true}, \tag{IV.17}$$

which is in full terms

$$\mathbf{a}_{measured} = \mathbf{a}_{true} + \mathbf{b} + \begin{bmatrix} \Delta s_x & 0 & 0 \\ 0 & \Delta s_y & 0 \\ 0 & 0 & \Delta s_z \end{bmatrix} \mathbf{a}_{true} + \begin{bmatrix} 0 & \zeta & -\varepsilon \\ -\zeta & 0 & \delta \\ \varepsilon & -\delta & 0 \end{bmatrix} \mathbf{a}_{true} + \begin{bmatrix} 0 & \alpha & \beta \\ \alpha & 0 & \gamma \\ \beta & \gamma & 0 \end{bmatrix} \mathbf{a}_{true}, \tag{IV.18}$$

thus, including the bias, the scaling, the misalignment and the non-orthogonality of accelerometer axes. The shear, rotation and the scaling can be summarized in a calibration matrix

$$\mathbf{K} = \begin{bmatrix} 1 + \Delta s_x & \alpha + \zeta & \beta - \varepsilon \\ \alpha - \zeta & 1 + \Delta s_y & \gamma + \delta \\ \beta + \varepsilon & \gamma - \delta & 1 + \Delta s_z \end{bmatrix} = \begin{bmatrix} s_x & \alpha + \zeta & \beta - \varepsilon \\ \alpha - \zeta & s_y & \gamma + \delta \\ \beta + \varepsilon & \gamma - \delta & s_z \end{bmatrix}. \tag{IV.19}$$

Keep in mind that the extension to a time-dependent scaling is given in equation IV.8. Multiplying the calibration to the signal in equation IV.4 and including the accelerometer bias $\mathbf{b}$ gives the observation equation with all instrument errors in SGG

$$\mathbf{a} = \mathbf{K}[(-\mathbf{T} + \mathbf{\Omega} + \dot{\mathbf{\Omega}})\mathbf{r}] + \mathbf{b} \tag{IV.20}$$

or written out in full for one accelerometer

$$\begin{aligned} \begin{bmatrix} a_x \\ a_y \\ a_z \end{bmatrix} = \begin{bmatrix} b_x \\ b_y \\ b_z \end{bmatrix} + \begin{bmatrix} s_x & \alpha + \zeta & \beta - \varepsilon \\ \alpha - \zeta & s_y & \gamma + \delta \\ \beta + \varepsilon & \gamma - \delta & s_z \end{bmatrix} \cdot \\ \left(\left(- \begin{bmatrix} V_{xx} & V_{xy} & V_{xz} \\ V_{yx} & V_{yy} & V_{yz} \\ V_{zx} & V_{zy} & V_{zz} \end{bmatrix} + \begin{bmatrix} -\omega_y^2 - \omega_z^2 & \omega_x\omega_y & \omega_x\omega_z \\ \omega_x\omega_y & -\omega_x^2 - \omega_z^2 & \omega_y\omega_z \\ \omega_x\omega_z & \omega_y\omega_z & -\omega_x^2 - \omega_y^2 \end{bmatrix} + \begin{bmatrix} 0 & -\dot{\omega}_z & \dot{\omega}_y \\ \dot{\omega}_z & 0 & -\dot{\omega}_x \\ -\dot{\omega}_y & \dot{\omega}_x & 0 \end{bmatrix} \right) \cdot \\ \begin{bmatrix} r_x \\ r_y \\ r_z \end{bmatrix} \Bigg). \end{aligned} \tag{IV.21}$$

The incorporation of the quadratic factor into the observation equation, is to be found in equation IV.16. Right now the observation equation does not include any forces acting on the satellite except the gravity and the apparent forces due to the system itself. All non-conservative forces resulting in friction, such as the atmospheric drag, are not considered yet. For that, the common mode accelerations $\mathbf{c}$ are added to the

signal, containing information about those forces, i.e. the linear acceleration of the CoM. A more detailed explanation why the common mode accelerations coincide with the linear acceleration in the CoM can be found in Siemes (2011).
In a system without external forces all common mode accelerations are zero, see Stummer (2006) and Siemes (2011). This state is the goal of the drag-free control system, meaning that that the magnitude of the external forces acting on the gradiometer is to be reduced. The common mode accelerations are the main input for this system. Even though the control systems tries to compensate the effect of the common mode accelerations, they have to be considered in the processing later on.
Including the non-conservative forces, equation IV.21 changes to

$$\begin{bmatrix} a_x \\ a_y \\ a_z \end{bmatrix} = \begin{bmatrix} b_x \\ b_y \\ b_z \end{bmatrix} + \begin{bmatrix} s_x & \alpha+\zeta & \beta-\varepsilon \\ \alpha-\zeta & s_y & \gamma+\delta \\ \beta+\varepsilon & \gamma-\delta & s_z \end{bmatrix} \cdot \left(\left(- \begin{bmatrix} V_{xx} & V_{xy} & V_{xz} \\ V_{yx} & V_{yy} & V_{yz} \\ V_{zx} & V_{zy} & V_{zz} \end{bmatrix} + \begin{bmatrix} -\omega_y^2-\omega_z^2 & \omega_x\omega_y & \omega_x\omega_z \\ \omega_x\omega_y & -\omega_x^2-\omega_z^2 & \omega_y\omega_z \\ \omega_x\omega_z & \omega_y\omega_z & -\omega_x^2-\omega_y^2 \end{bmatrix} + \begin{bmatrix} 0 & -\dot{\omega}_z & \dot{\omega}_y \\ \dot{\omega}_z & 0 & -\dot{\omega}_x \\ -\dot{\omega}_y & \dot{\omega}_x & 0 \end{bmatrix} \right) \cdot \begin{bmatrix} r_x \\ r_y \\ r_z \end{bmatrix} + \begin{bmatrix} c_x \\ c_y \\ c_z \end{bmatrix} \right) \quad \text{(IV.22)}$$

or short

$$\mathbf{a} = \mathbf{K}[(-\mathbf{T} + \mathbf{\Omega} + \dot{\mathbf{\Omega}})\mathbf{r} + \mathbf{c}] + \mathbf{b}, \quad \text{(IV.23)}$$

providing a full connection between the accelerations measured on the left hand side and all parameters affecting the observations including the gravity field parameters in the tensor $\mathbf{T}$. Note that this equation is only valid with respect to the GRF.

3 HPF approach

The approach developed within the HPFs can be divided into five parts. By merging the observed accelerations in certain linear combinations, it is possible to derive the gravity gradient components as well as the perturbing angular accelerations and common mode accelerations. A detailed explanation can be found in Stummer (2006) and Siemes (2011).

Step 1: Starting from the observation equation of SGG but omitting the errors

$$\mathbf{a} = (-\mathbf{T} + \mathbf{\Omega} + \dot{\mathbf{\Omega}})\mathbf{r} + \mathbf{c} \quad \text{(IV.24)}$$

the common mode acceleration $\mathbf{c}$ can be calculated by averaging the measurements along one gradiometer arm

$$2a_{c,1,4,x} = a_{1,x} + a_{4,x}, \quad \text{(IV.25)}$$

$$2a_{c,1,4,y} = a_{1,y} + a_{4,y}, \quad \text{(IV.26)}$$

$$\vdots$$

As the GOCE moves in a system with external influences, the measured accelerations have to be corrected by the common mode accelerations.
Next, the differential mode accelerations are computed with the linear combination of

$$a_{d,1,4,x} = a_{1,x} - a_{4,x} = (-V_{xx} - \omega_y^2 - \omega_z^2)L_x, \tag{IV.27}$$
$$a_{d,1,4,y} = a_{1,y} - a_{4,y} = (-V_{zx} - \dot{\omega}_z + \omega_x\omega_y)L_x, \tag{IV.28}$$
$$a_{d,1,4,z} = a_{1,z} - a_{4,z} = (-V_{zx} - \dot{\omega}_y + \omega_x\omega_z)L_x, \tag{IV.29}$$
$$a_{d,2,5,x} = a_{2,x} - a_{5,x} = (-V_{xy} - \dot{\omega}_z + \omega_x\omega_y)L_y, \tag{IV.30}$$
$$a_{d,2,5,y} = a_{2,y} - a_{5,y} = (-V_{yy} - \omega_x^2 - \omega_z^2)L_y, \tag{IV.31}$$
$$a_{d,2,5,z} = a_{2,xz} - a_{5,z} = (-V_{zy} + \dot{\omega}_x + \omega_x\omega_z)L_y, \tag{IV.32}$$
$$a_{d,3,6,x} = a_{3,x} - a_{6,x} = (-V_{xz} - \dot{\omega}_y + \omega_x\omega_z)L_z, \tag{IV.33}$$
$$a_{d,3,6,y} = a_{3,y} - a_{6,y} = (-V_{yz} - \dot{\omega}_x + \omega_y\omega_z)L_z, \tag{IV.34}$$
$$a_{d,36,z} = a_{3,z} - a_{6,z} = (-V_{zz} - \omega_x^2 - \omega_y^2)L_z, \tag{IV.35}$$

linking the observed accelerations directly with the quantities of the gravity field. From this equation, the tensor components can be expressed directly, however, the centrifugal and Euler forces are still unknown.
Fortunately, the angular accelerations have a linear relation with the differential mode accelerations and the length of the respective gradiometer arm

$$\dot{\omega}_x = -\frac{a_{d,3,6,y}}{L_z} + \frac{a_{d,2,5,z}}{L_y}, \tag{IV.36}$$

$$\dot{\omega}_y = -\frac{a_{d,1,4,z}}{L_x} + \frac{a_{d,3,6,x}}{L_z}, \tag{IV.37}$$

$$\dot{\omega}_z = \frac{a_{d,1,4,y}}{L_x} - \frac{a_{d,2,5,x}}{L_y}. \tag{IV.38}$$

As one axis of each accelerometer was weaker than the two others, the arrangement of the six accelerometers is chosen such as to permit most accurate determination of $\dot{\omega}_y$, whereas $\dot{\omega}_x$ and $\dot{\omega}_z$ are not determined that well. Therefore, T_{xx}, T_{yy}, T_{zz} and T_{xz} can be calculated with highest precision [Stummer (2006)].

Step 2: For deriving the gradient, only the angular rates are missing. They can be determined in two ways: Either by differentiating the attitude quaternion from the star trackers to angular velocities or by integrating the above calculated angular accelerations

$$\omega(t) = \int_{t_0}^{t} \dot{\omega}(t)dt + \omega_0. \tag{IV.39}$$

As mentioned earlier, the noise characteristics of the EGG and the star sensors are opposite. Including the noise propagation by differentiation the star sensor is more accurate in the low frequencies, whereas the EGG can be used for the calculation of the faster oscillating components of ω. The combination of the two instruments to compute the angular rate is called angular rate reconstruction. This processing step tries to combine the star sensor and gradiometer data in an optimal way [Siemes (2011)], simplified it is a low-pass filtered solution of the star tracker's data to support the low frequencies and a high-pass filtered integration of the above mentioned linear combinations (equation IV.36, IV.37 and IV.38), which provides best information

in the high frequencies.

$$\omega = \text{lowpass}(\omega^{\text{StarTracker}}) + \text{highpass}(\omega^{EGG}) \tag{IV.40}$$

According to Siemes (2011) the high-pass filter is optimal designed when eliminating the integration constant ω_0 that occurs within the integration in equation IV.39. The filtering itself is done in a Wiener filter approach, where the attitude and the angular accelerations are merged based on their accuracy, which is frequency dependent, see Stummer et al. (2011).

Step 3: The unknown calibration matrix $\mathbf{K}$ is determined through satellite shaking. The correct calibration of the common mode accelerations and differential mode accelerations is crucial for the HPF approach.

Step 4: Short rearranging leads to the expression of the gradient with respect to the GRF.

$$V_{xx} = -2\frac{a_{d,1,4,x}}{L_x} - \omega_y^2 - \omega_z^2 \tag{IV.41}$$

$$V_{yy} = -2\frac{a_{d,2,5,y}}{L_y} - \omega_x^2 - \omega_z^2 \tag{IV.42}$$

$$V_{zz} = -2\frac{a_{d,3,6,z}}{L_z} - \omega_x^2 - \omega_y^2 \tag{IV.43}$$

$$V_{xy} = -\frac{a_{d,2,5,x}}{L_y} - \frac{a_{d,1,4,y}}{L_x} + \omega_x\omega_y \tag{IV.44}$$

$$V_{xz} = -\frac{a_{d,1,4,z}}{L_x} - \frac{a_{d,3,6,x}}{L_z} + \omega_x\omega_z \tag{IV.45}$$

$$V_{yz} = -\frac{a_{d,3,6,y}}{L_z} - \frac{a_{d,2,5,z}}{L_y} + \omega_y\omega_z \tag{IV.46}$$

Even though there are only five independent tensor element, six are calculated ($V_{xx}, V_{yy}, V_{zz}, V_{xy}, V_{xz}, V_{yz}$). These gradients are given in Level 1b data including the rotation from GRF to IRF.
Consequently, the gravity gradients are rotated into the IRF.

Step 5: The gravity gradients are introduced in a least squares adjustment as observations to estimate the coefficients of a spherical harmonic expansion.

Part V

The raw accelerometer data approach (RADA)

The raw accelerometer data approach starts with the idea of linking all observations directly with the parameters that need to be known to estimate an accurate gravity field. All linear combinations, such as the differential mode accelerations, the common mode accelerations and reconstructions, shall be avoided. Thus, the observation equation (equation IV.22) including all errors has to be used directly for the evaluation.

The unknown quantities are the coefficients of a spherical harmonic expansion of the Earth's gravity field, the angular rates and accelerations (or at least one of them, since they are related directly be integration or differentiation), the common mode accelerations, the length of the gradiometer arms, the scale in a linear approach and the bias of the accelerometers (see the full observation equation in the last chapter, equation IV.22). Additionally the quadratic behaviour of the signal is considered.
The measurements are three accelerations from six accelerometers per epoch, making 18 observations and 4 attitude quaternion components derived from the star trackers, also given at every epoch.
Generally spoken, the problem can be written as

$$\mathbf{l} = \mathbf{A}\mathbf{x} + \mathbf{e}. \tag{V.1}$$

Here $\mathbf{l}$ contains all observations, $\mathbf{A}$ is a design matrix forming a relation between the left hand side and the unknown parameters in $\mathbf{x}$. The vector $\mathbf{e}$ denotes the residuals or errors between the observations $\mathbf{l}$ and the mathematical formulation for the observations $\mathbf{Ax}$. It follows a Gaussian distribution. The observations contain, as already mentioned, 22 measurements per epoch, thus resulting in around 500 million data points. The unknown quantities sum up to roughly 200 million, leaving over-determined simultaneous equations. Hence, the solving is done in a least squares adjustment. The estimation of unknown parameters in a least squares adjustment follows

$$\hat{\mathbf{x}} = (\mathbf{A}^T\mathbf{P}\mathbf{A})^{-1}\mathbf{A}^T\mathbf{P}\mathbf{l}, \tag{V.2}$$

with $\hat{\mathbf{x}}$ denoting the estimated parameters. $\mathbf{P}$ gives the weighting of each observation introducing possible random uncertainties. The weight is connected to the variance with

$$p_i = \frac{1}{\sigma^2_{observation}}. \tag{V.3}$$

$\mathbf{P}$ can be either a diagonal or a fully populated matrix.
The components $(\mathbf{A}^T\mathbf{P}\mathbf{A})$ and $\mathbf{A}^T\mathbf{P}\mathbf{l}$ describe the normal equations $\mathbf{N}$ and the right hand side of the normal equations $\mathbf{n}$ respectively. Thus, the system may be written as

$$\hat{\mathbf{x}} = \mathbf{N}^{-1}\mathbf{n}. \tag{V.4}$$

Via the inverse of the normal equations the variance/-covariance matrix of $\hat{\mathbf{x}}$ is obtained.

$$\mathbf{C}_{\hat{\mathbf{x}}} = \mathbf{N}^{-1} = (\mathbf{A}^T\mathbf{P}\mathbf{A})^{-1}. \tag{V.5}$$

As the statement of the problem contains many of different parameters, they can be divided into four groups: First the parameters that have to be determined in every single epoch, i.e. the angular rates and/or the angular accelerations and the common mode accelerations. Second, the parameters which are sought-after per orbit arc. Third, quantities to be estimated monthly (i.e. calibration parameters) and last parameters to be determined on a global level over the whole time span. Table V.1 gives a list of the parameters in the raw accelerometer data approach and their assignment to one of the groups. The number in the brackets gives the amount in the respective time span.

Table V.1: Parameters of the RADA

per epoch	#	**per arc**	#	**per month**	#	**global**	#
angular acc.	(3)	bias	(18)	constant scaling	(54)	gravity field	d/o 250:
common mode acc.	(3)	start rate &	(3)	linear scaling	(54)	coefficients	62997
		quaternion	(4)	k_2 factor	(18)		
				length of			
				gradiometer arms	(18)		

In order to provide enough information for the whole evaluation, the computation is done on a monthly level. Each month is divided into short arcs of 15 minutes. For a sampling of 5 seconds, this sums up to 180 epochs per arc, which are 3960 observations in $\mathbf{l}$. The longer the arc, the bigger the normal equations get and the more (fast accessible) memory is necessary, which increases the calculation time. Too short arcs do not provide enough information for the bias.

Within the design matrix, the problem was divided into two parts

$$\mathbf{l} = \begin{bmatrix} \mathbf{A} & \mathbf{B} \end{bmatrix} \begin{bmatrix} \mathbf{x}_{long-term} \\ \mathbf{x}_{short-term} \end{bmatrix}. \tag{V.6}$$

Part $\mathbf{A}$ of the design matrix contains the relation to all parameters of monthly or global interest. $\mathbf{B}$ takes the short term quantities into account. The short term parameters in $\mathbf{B}$ were built up for one arc and then eliminated on the level of observation equation. This means, there are $(3^{common\,mode\,acc.} + 3^{ang.\,acc.}) \cdot 180^{epochs} + 3^{start\,ang.\,rate} + 4^{start\,quaternion} + 18^{bias} = 1105$ parameters to estimate. However, the bias was not formulated as a constant, but rather with a time depending Legendre polynomial of degree two, the number of unknown parameters is a bit higher.

The quantities in $\mathbf{A}$ are calculated monthly for the calibration parameters. By accumulating the monthly normal equations, the global gravity field coefficients, also part of $\mathbf{A}$, are obtained. Then the monthly parameters are eliminated on normal equation level. Summing up all parameters in $\mathbf{A}$ except the gravity field coefficients, 144 calibration parameters are represented. However, as the scaling and the length of the gradiometer arms are linearly dependent, a rank deficiency of four occurs (the centre of the coordinate system can be moved in x, y, z and a scale factor can be applied, since doubling the calibration scale factors results in halving the gradiometer arm lengths). Therefore, the datum is chosen via re-parametrization of the positions on the mean positions of the accelerometers, leading to 140 independent unknown parameters for the calibration. When the spherical harmonic expansion is truncated at degree and order (d/o) 250, as it was done for this thesis, 62997 unknown coefficients are part of $\mathbf{A}$ as well.

1 EGG observations

The observations from the EGG instrument are 18 accelerations per epoch measured with the six accelerometers, leading to 3240 observations per arc. Since the relation given in equation V.6 is linear, either a linear relation between the observations and the unknown parameters has to be found or a linearisation has to be applied. To simplify matters, equation IV.22 may be written as

$$\mathbf{a} = \mathbf{K}[(-\mathbf{T} + \mathbf{\Omega} + \dot{\mathbf{\Omega}})\mathbf{r} + \mathbf{c}] + \mathbf{b} \tag{V.7}$$

formulating a relation between one accelerometer with the measurements $\mathbf{a} = \begin{bmatrix} a_x & a_y & a_z \end{bmatrix}^T$ and the unknown parameters on the right hand side. $\mathbf{K}$ is the calibration matrix including the scale factor, misalignment and non-orthogonality of the accelerometer axes, $\mathbf{T}$ denotes the gravity tensor and $\mathbf{\Omega}$ and $\dot{\mathbf{\Omega}}$ are the angular rates and angular accelerations respectively as well as $\mathbf{r}$ as a vector containing the accelerometer positions in the GRF. $\mathbf{c}$ gives the common mode accelerations and $\mathbf{b}$ is the accelerometer bias.
The inner term in the GRF without the errors may be introduced as

$$\mathbf{M} = -\mathbf{T} + \mathbf{\Omega} + \dot{\mathbf{\Omega}} \tag{V.8}$$

and the signal as

$$\mathbf{S} = \mathbf{M}\mathbf{r} + \mathbf{c} \tag{V.9}$$

which leads for equation V.7 to the notation

$$\mathbf{a} = \mathbf{K}(\mathbf{M}\mathbf{r} + \mathbf{c}) + \mathbf{b} \tag{V.10}$$

and further to

$$\mathbf{a} = \mathbf{K}\mathbf{S} + \mathbf{b}. \tag{V.11}$$

As it can be seen easily, the formal relation is not linear for every parameter. Consequently, a linearisation with a truncated Taylor series is applied. Since Taylor series demand a good approximation point, another model, the GOCO05s as one of the most accurate global satellite-only gravity field models, is introduced and taken as Taylor point. The orbital positions were computed from GPS data in a Reduced Dynamic Orbit, since the locating of the measurements is necessary. Approximations for the angular rate and the angular acceleration are derived from the attitude quaternion.

1.1 Parametrization of the short-term components

The derivations for the linearisation of the short-term quantities in $\mathbf{B}$ come up with a problem between the bias and the common mode accelerations, since both act in the same way within the mathematical model (see equation V.10). The bias' relation is linear, even though a Legendre polynomial was used for modelling. Also the common mode accelerations are linear, depending only on the calibration matrix.

$$\frac{\partial \mathbf{a}}{\partial \mathbf{b}} = 1 = \text{coeff. for Legendre polynomial} \tag{V.12}$$

and

$$\frac{\partial \mathbf{a}}{\partial \mathbf{c}} = \frac{\partial \mathbf{a}}{\partial \mathbf{S}} \frac{\partial \mathbf{S}}{\partial \mathbf{c}} = \mathbf{K}\mathbf{I}. \tag{V.13}$$

Therefore, the signal from the common mode accelerations cannot be separated from the bias strictly. In this approach, a QR-decomposition between the bias and the common mode accelerations is used, leaving every signal, that is physically unaccountable in the null space. Thus, the bias absorbs those signals. For the common mode accelerations, only the unity component $\mathbf{I}$ is used, for the bias the Legendre polynomial.

The parametrization of the angular accelerations is a difficult task, since they occur in every component of the inner term $\mathbf{M}$. Repeating

$$\mathbf{M} = -\mathbf{T}+\mathbf{\Omega}+\dot{\mathbf{\Omega}} = -\begin{bmatrix} V_{xx} & V_{xy} & V_{xz} \\ V_{yx} & V_{yy} & V_{yz} \\ V_{zx} & V_{zy} & V_{zz} \end{bmatrix} + \begin{bmatrix} -\omega_y^2-\omega_z^2 & \omega_x\omega_y & \omega_x\omega_z \\ \omega_x\omega_y & -\omega_x^2-\omega_z^2 & \omega_y\omega_z \\ \omega_x\omega_z & \omega_y\omega_z & -\omega_x^2-\omega_y^2 \end{bmatrix} + \begin{bmatrix} 0 & -\dot{\omega}_z & \dot{\omega}_y \\ \dot{\omega}_z & 0 & -\dot{\omega}_x \\ -\dot{\omega}_y & \dot{\omega}_x & 0 \end{bmatrix} \tag{V.14}$$

shows that the angular accelerations occur in the last component directly, but also $\mathbf{T}$ and $\mathbf{\Omega}$ are dependent from $\dot{\omega}$. Since the angular rates have to be considered as well, the relation to the angular acceleration, which are estimated in the least squares adjustment, is the integral within two epochs, written as

$$\omega(t) = \int_{t_0}^{t} \dot{\omega}(t)dt + \omega_0 \tag{V.15}$$

with a start angular rate ω_0. Also the tensor depends on the angular acceleration because of a rotation from the IRF to the GRF

$$\mathbf{T}_{GRF} = \mathbf{R}^T\mathbf{T}_{IRF}\mathbf{R}. \tag{V.16}$$

As it has to be done with the approximate values, the tensor contains the attitude quaternion, which is the twofold integration of the angular acceleration.

$$\mathbf{q}(t) = \int_{t_0}^{t} \dot{\mathbf{q}}(t)dt + \mathbf{q}_0 \tag{V.17}$$

with the start quaternion $\mathbf{q}_0$ and

$$\dot{\mathbf{q}} = \begin{bmatrix} \dot{q}_0 \\ \dot{q}_x \\ \dot{q}_y \\ \dot{q}_z \end{bmatrix} = \frac{1}{2}\begin{bmatrix} q_x & q_y & q_z \\ -q_0 & -q_z & q_y \\ q_z & -q_0 & -q_x \\ -q_y & q_y & -q_0 \end{bmatrix}\begin{bmatrix} \omega_x \\ \omega_y \\ \omega_z \end{bmatrix}.$$

The angular rates are still calculated via equation V.15. Therefore, the derivation of $\frac{\partial \mathbf{a}}{\partial \dot{\omega}}$ consists of three parts, which have to be accumulated. The last component my be written as

$$\frac{\partial \mathbf{a}}{\partial \dot{\omega}} = \frac{\partial \mathbf{a}}{\partial \mathbf{S}}\frac{\partial \mathbf{S}}{\partial \dot{\omega}} = \mathbf{K}\begin{bmatrix} \frac{\partial \mathbf{S}}{\partial \dot{\omega}_x} & \frac{\partial \mathbf{S}}{\partial \dot{\omega}_y} & \frac{\partial \mathbf{S}}{\partial \dot{\omega}_z} \\ \downarrow & \downarrow & \downarrow \\ 0 & r_z & -r_y \\ -r_z & 0 & r_x \\ r_y & -r_x & 0 \end{bmatrix}. \tag{V.18}$$

The parametrization of the second component is

$$\frac{\partial \mathbf{a}}{\partial \dot{\omega}} = \frac{\partial \mathbf{a}}{\partial \mathbf{S}} \frac{\partial \mathbf{S}}{\partial \omega} \frac{\partial \omega}{\partial \dot{\omega}}, \tag{V.19}$$

written in full

$$\frac{\partial \mathbf{a}}{\partial \omega} = \frac{\partial \mathbf{a}}{\partial \mathbf{S}} \frac{\partial \mathbf{S}}{\partial \omega} = \mathbf{K} \begin{bmatrix} \frac{\partial \mathbf{S}}{\partial \omega_x} \downarrow & \frac{\partial \mathbf{S}}{\partial \omega_y} \downarrow & \frac{\partial \mathbf{S}}{\partial \omega_z} \downarrow \\ \omega_y r_y + \omega_z r_z & -2\omega_y r_x + \omega_x r_y & -2\omega_z r_x + \omega_x r_z \\ -2\omega_x r_y + \omega_y r_x & \omega_x r_x + \omega_z r_z & -2\omega_z r_y + \omega_y r_z \\ -2\omega_x r_z + \omega_z r_x & -2\omega_y r_z + \omega_z r_y & \omega_x r_x + \omega_y r_y \end{bmatrix} \tag{V.20}$$

and

$$\frac{\partial \omega}{\partial \dot{\omega}} = \frac{\partial}{\partial \dot{\omega}} \int_{t_0}^{t} \dot{\omega}(t) dt + \omega_0, \tag{V.21}$$

meaning that $\omega = \dot{\omega} \cdot \frac{\partial}{\partial \dot{\omega}} \int_{t_0}^{t} \dot{\omega}(t) dt + \omega_0$. The derivation for the first component reads as

$$\frac{\partial \mathbf{a}}{\partial \dot{\omega}} = \frac{\partial \mathbf{a}}{\partial \mathbf{S}} \frac{\partial \mathbf{S}}{\partial \mathbf{R}} \frac{\partial \mathbf{R}}{\partial \mathbf{q}} \frac{\partial \mathbf{q}}{\partial \omega} \frac{\partial \omega}{\partial \dot{\omega}}, \tag{V.22}$$

with $\frac{\partial \mathbf{S}}{\partial \mathbf{R}}$ given due to its length in pseudo code as

```
dim(dSdR) = (3,9)
R = {R11, R12, R13;
     R21, R22, R23;
     R31, R32, R33};
T = {Vxx, Vxy, Vxz;
     Vxy, Vyy, Vyz;
     Vxz, Vyz, Vzz};
position = {rx;
            ry;
            rz};
for r1 = 0:2
    for c1 = 0:2
        for r2 = 0:2
            for c2 = 0:2
                dSdR(r1,3*r1+r2) -= T(r2,c2)*position(c1)*R(c1,c2);
                dSdR(r1,3*c1+c2) -= T(r2,c2)*position(c1)*R(r1,r2);
            end
        end
    end
end
```

and

$$\frac{\partial \mathbf{R}}{\partial \mathbf{q}} = \begin{bmatrix} \frac{\partial \mathbf{R}}{\partial q_0} \downarrow & \frac{\partial \mathbf{R}}{\partial q_x} \downarrow & \frac{\partial \mathbf{R}}{\partial q_y} \downarrow & \frac{\partial \mathbf{R}}{\partial q_z} \downarrow \\ 2q_0 & 2q_x & -2q_y & -2q_z \\ -2q_z & 2q_y & 2q_x & -2q_0 \\ 2q_y & 2q_z & 2q_0 & 2q_x \\ 2q_z & 2q_y & 2q_x & 2q_0 \\ 2q_0 & -2q_x & 2q_y & -2q_z \\ -2q_x & -2q_0 & 2q_z & 2q_y \\ -2q_y & 2q_z & -2q_0 & 2q_x \\ 2q_x & 2q_0 & 2q_z & 2q_y \\ 2q_0 & -2q_x & -2q_y & 2q_z \end{bmatrix}. \tag{V.23}$$

The last term $\frac{\partial \mathbf{q}}{\partial \omega}\frac{\partial \omega}{\partial \dot{\omega}}$ is the integral from angular accelerations to quaternions, thus being a twofold integration, where the second component is given in equation V.21 and the first one can be obtained via equation V.17.

$$\frac{\partial \mathbf{q}}{\partial \omega}\frac{\partial \omega}{\partial \dot{\omega}} = \frac{\partial \omega}{\partial \dot{\omega}} \left\{ \int_{t_0}^{t} \frac{1}{2} \begin{bmatrix} q_x & q_y & q_z \\ -q_0 & -q_z & q_y \\ q_z & -q_0 & -q_x \\ -q_y & q_y & -q_0 \end{bmatrix}_{(t)} \left(\int_{t_0}^{t} \dot{\omega}(t)dt + \omega_0 \right) dt + \mathbf{q}_0 \right\}. \tag{V.24}$$

Again $\mathbf{q} = \dot{\omega} \cdot \frac{\partial \mathbf{q}}{\partial \omega}\frac{\partial \omega}{\partial \dot{\omega}}$.
Summing up those three parts and factorising $\frac{\partial \mathbf{a}}{\partial \mathbf{S}} = \mathbf{K}$ it comes to

$$\frac{\partial \mathbf{a}}{\partial \dot{\omega}} = \mathbf{K}\left(\frac{\partial \mathbf{S}}{\partial \mathbf{R}}\frac{\partial \mathbf{R}}{\partial \mathbf{q}}\frac{\partial \mathbf{q}}{\partial \omega}\frac{\partial \omega}{\partial \dot{\omega}} + \frac{\partial \mathbf{S}}{\partial \omega}\frac{\partial \omega}{\partial \dot{\omega}} + \frac{\partial \mathbf{S}}{\partial \dot{\omega}}\right). \tag{V.25}$$

1.2 Parametrization of the long-term components

The derivation for the position is after the elimination of the rank deficiency simply

$$\frac{\partial \mathbf{a}}{\partial \mathbf{r}} = \frac{\partial \mathbf{a}}{\partial \mathbf{S}}\frac{\partial \mathbf{S}}{\partial \mathbf{r}} = \mathbf{KM}. \tag{V.26}$$

The parametrization for the other calibration parameters is linear both for the constant part and the trend

$$\frac{\partial \mathbf{a}}{\partial \mathbf{K}_{const.}} = \mathbf{S} \quad \text{and} \quad \frac{\partial \mathbf{a}}{\partial \mathbf{K}_{trend.}} = \mathbf{S}(t - t_0). \tag{V.27}$$

For the quadratic term k_2 it comes to

$$\frac{\partial \mathbf{a}}{\partial k_{2.}} = \mathbf{S}^2. \tag{V.28}$$

For the tensor one condition can be added: The trace of the tensor becomes zero because the Laplace equation is fulfilled, see equation III.3.

$$\text{trace}(\mathbf{T}) = V_{xx} + V_{yy} + V_{zz} = 0, \tag{V.29}$$

so the tensor may be rewritten as

$$\mathbf{T} = \begin{bmatrix} V_{xx} & V_{xy} & V_{xz} \\ V_{yx} & V_{yy} & V_{yz} \\ V_{zx} & V_{zy} & -V_{xx} - V_{yy} \end{bmatrix} \tag{V.30}$$

For the five independent tensor elements, then the derivation becomes

$$\frac{\partial \mathbf{a}}{\partial \mathbf{T}_{GRF}} = \frac{\partial \mathbf{a}}{\partial \mathbf{S}}\frac{\partial \mathbf{S}}{\partial \mathbf{T}_{GRF}} = \mathbf{K} \begin{matrix} \frac{\partial \mathbf{S}}{\partial V_{xx}} \\ \downarrow \\ \end{matrix} \begin{matrix} \frac{\partial \mathbf{S}}{\partial V_{xy}} \\ \downarrow \\ \end{matrix} \begin{matrix} \frac{\partial \mathbf{S}}{\partial V_{xz}} \\ \downarrow \\ \end{matrix} \begin{matrix} \frac{\partial \mathbf{S}}{\partial V_{yy}} \\ \downarrow \\ \end{matrix} \begin{matrix} \frac{\partial \mathbf{S}}{\partial V_{yz}} \\ \downarrow \\ \end{matrix} \begin{bmatrix} -r_x & -r_y & -r_z & 0 & 0 \\ 0 & -r_x & 0 & -r_y & -r_z \\ r_z & 0 & -r_z & r_z & -r_y \end{bmatrix} \tag{V.31}$$

Note that the rotation from the EFRF to GRF has to be done here because the observation equation is only valid in the GRF, though the unknown tensor elements, which are then used for the spherical harmonic

expansion, are sought-after in the EFRF.

$$\mathbf{T}_{GRF} = \mathbf{R}\mathbf{T}_{EFRF}\mathbf{R}^T \tag{V.32}$$

leads to

$$\frac{\partial \mathbf{a}}{\partial \mathbf{T}_{EFRF}} = \frac{\partial \mathbf{a}}{\partial \mathbf{T}_{GRF}} \frac{\partial \mathbf{T}_{GRF}}{\partial \mathbf{T}_{EFRF}}. \tag{V.33}$$

2 Star tracker observations

As one attitude quaternion per epoch is measured, 720 additional observations per arc are introduced from the star trackers. The parametrization of the star camera observations only affects the estimation of the angular accelerations, since there is no other relation between the attitude and the other unknown parameters. The derivation is

$$\frac{\partial \mathbf{q}}{\partial \dot{\omega}} = \frac{\partial \mathbf{q}}{\partial \omega} \frac{\partial \omega}{\partial \dot{\omega}}, \tag{V.34}$$

which is already known from equation V.24. Within the raw accelerometer data approach, the star tracker data shall support the accurate estimation of the angular accelerations. The weight of these measurements is chosen higher to support the low frequencies, in which the gradiometer is weaker as it covers mostly medium to short wavelengths.

3 Implementation and settings

Following the theory of the raw accelerometer data approach, this chapter describes the implementation and the necessary settings for the computation.

Implementation

With the knowledge of the parametrization, the observation equations can be built. Due to computation time issues the whole processing was divided into two separate parts, one part for the preprocessing and the processing step for calculation of the gravity field coefficients.

As the statement of the problem contains not only linear components, the linearisation through the truncated Taylor series demands an accurate Taylor point. Within the preprocessing step another gravity field model, the aforementioned GOCO05s, is introduced as Taylor point. This step determines all parameters in a least squares adjustment except the gravity field coefficients. It is set up iteratively, meaning that the Taylor point is improved with the solution in every iteration. The iteration stops when convergence is reached, i.e. the solution differs from the Taylor point insignificantly.
Considering the random noise, the weighting of the observations is done using a Variance Component Estimation (VCE), since the numerous number of observations would otherwise lead to a too large weight matrix $\mathbf{P}$ in the least squares adjustment.
The VCE affords the possibility to subsume observations to groups and computing a variance for each group. This is done individually for each arc, axis and accelerometer and the star camera observations of an arc. The variance component estimation makes it possible to omit any outlier detection beforehand, since arcs with bad data quality receive a low weight. Assumptions for the VCE are

- independent accelerometer axes, as one variance per axis is estimated,
- independent arcs and
- a stationary process, i.e. the statistical moments do not change in time.

The variance can be expressed in a covariance function as well, which indicates the variance in dependency of time. For an arc length of 15 minutes and a 5 second sampling one arc gives a resolution of 180 epochs. As the arcs are considered being independent, $180 \cdot 5\,\mathrm{s} = 900\,\mathrm{s} = 15\,\mathrm{min}$ is the maximum length of the covariance function, thus, all observations further afar are not considered as being correlated. In order to give the errors with respect to the frequency the covariance function can be transformed into a Power Spectral Density (PSD) using Fourier transformation. Figure V.1 gives the Power Spectral Density for three months, one at the beginning of the observations (November 2009, upper left graph), one for dense data towards the end of GOCE (January 2013, upper right chart) and one for sparse data towards the end of the mission (May 2013, lower right diagram).

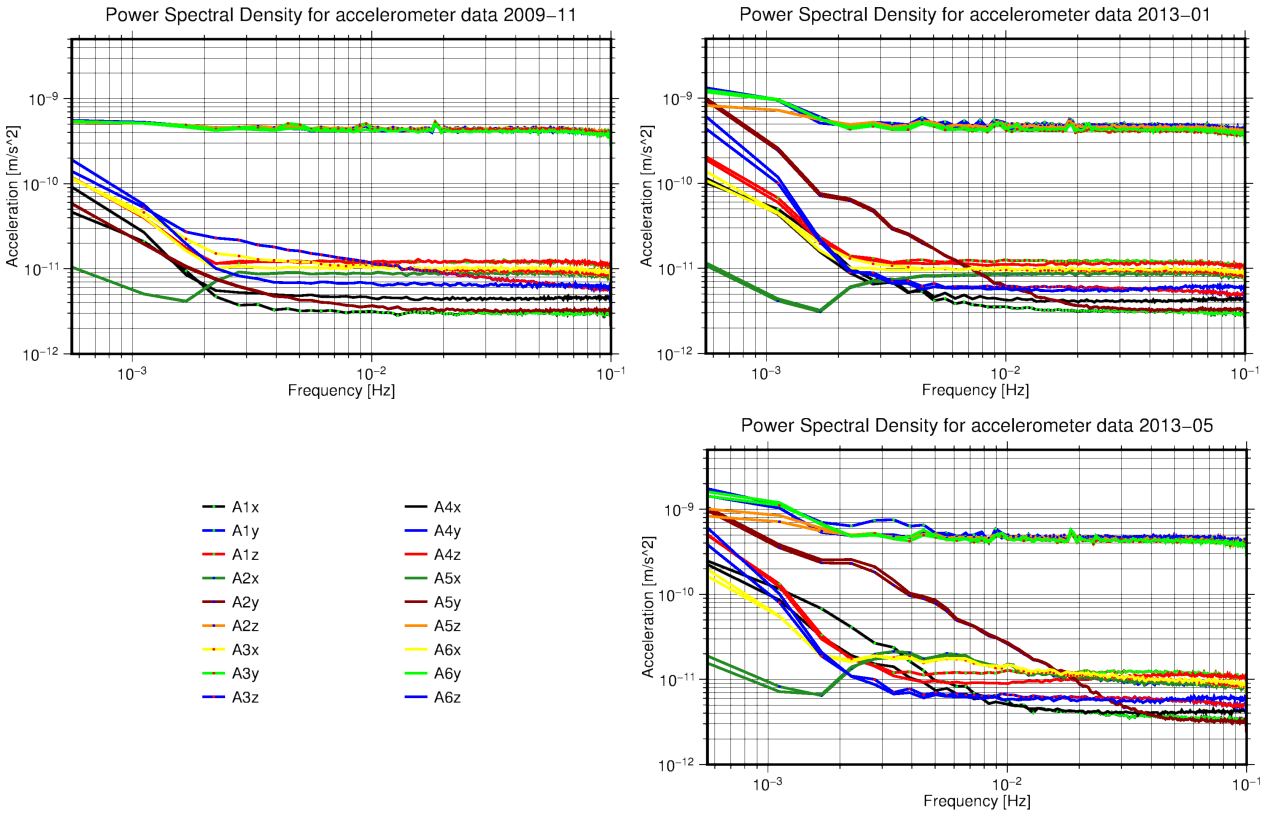

Figure V.1: Power Spectral Density of accelerometer observations

The different sensitivity of the axes classifies two groups in the observations. However, the two axes A2y and A5y, which are high sensitive on the across track axis of the gradiometer show a higher variance over time. This effect may be ascribed to the geomagnetic equator as this axis is used to compute the differential mode accelerations for the V_{yy} component, which seems to follow the geomagnetic equator, see Siemes (2017). Reducing this effect may help improving GOCE data processing.

The values from the preprocessing are saved in external files. These are improved star tracker observations, common mode accelerations, calibration parameters and a covariance function for the weighting.

These improved quantities are then introduced in the processing step as approximate values for the actual calculation of the gravity field coefficients. Here, the observation equation is the same as in the preprocessing step, not excluding the gravity field parameters, but omitting the iteration. For the least squares adjustment the observation equation is solved using all observations from the gradiometer and the star camera. The random noise in the measurements is modelled with the covariance function from the preprocessing.
Until now, only the gravity tensor elements were introduced as unknown parameters. For the processing step they are expanded in a spherical harmonic series with coefficients c_{nm} and s_{nm}, which are then estimated.

As the GOCE mission provides 47 months of data for the EGG instrument, every month was processed individually and the normal equations were accumulated to obtain a solution for the static gravity field. A regularization according to Kaula's rule was added afterwards.

Settings for the RADA

The approach of processing the EGG data chosen in the RADA is quite flexible towards changes in the parameters. Therefore, three months were selected to test different settings. In order to pick representative test data, one month at the beginning (November 2009), providing a full month of observations, was taken into account. Here, problems, such as a quadratic signal behaviour, do not occur. To investigate poor data conditions the month May 2013 was chosen, in which a lot of data is missing and the signal-to-voltage conversion got worse. The third month chosen is January 2013, also containing a full month of observations, but close to the mission's end (see the Power Spectral Densities in figure V.1). The examination whether interim results are realistic and leading to a gravity field was carried out in comparison of, for instance, the estimated common mode accelerations to the ones given in the Level 1b data.
While keeping an eye on the calculation time and the crucial determination of the bias, arcs of 15 minutes were an appropriate choice. Arcs, which are too short distort the long wavelengths when the bias degree is set higher than two, arcs that are too long consume significantly more computation time. Directly connected to the arc length is the bias degree: The shorter the arc, the lower the degree has to be in order to avoid any oscillations. For arcs of 15 minutes a Legendre polynomial of degree two is adequate. Since the bias is estimated for each arc, a jump discontinuity between the arcs occurs, the magnitude depends on the bias degree. A higher bias degree, which is only possible with longer arcs, seems to interact better with the time-varying quality of A2y and A5y measurements, absorbing more of the disturbance signal, but distorting the long wavelengths.
Figure V.2 shows a comparison between different arc lengths for the month 2013-01 up to a spherical harmonic degree of 180.

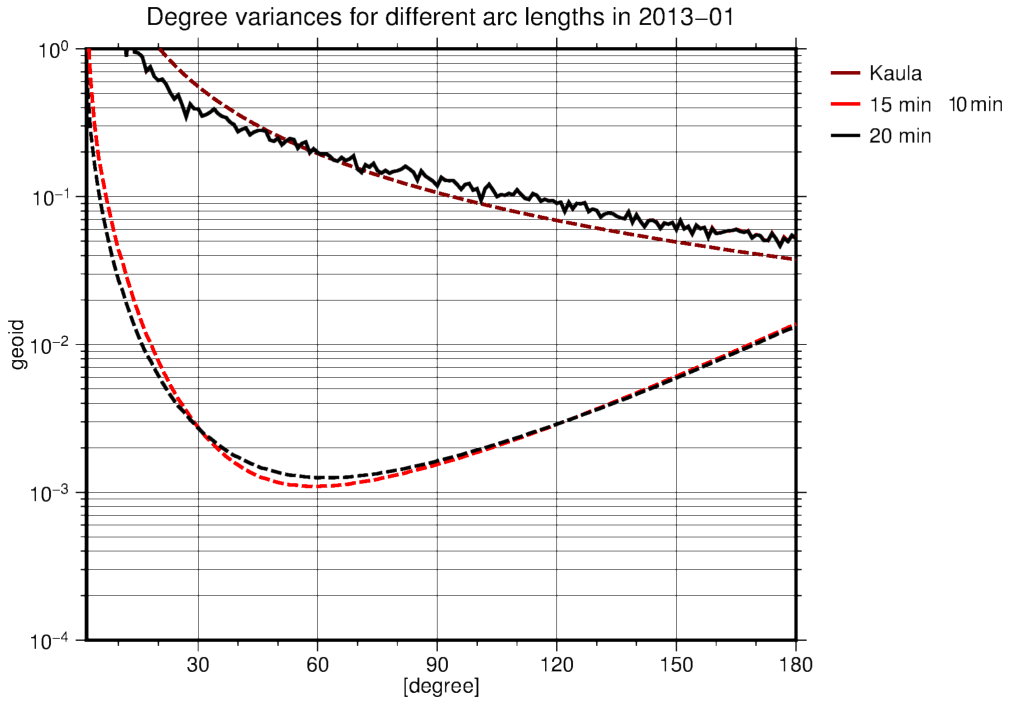

Figure V.2: Degree variances 2013-01 computed with different arc lengths and bias degrees

The test was executed for arcs of 10 minutes, 15 minutes and 20 minutes length with a bias degree of 2. Between the first two no difference can be stated, a small one occurs when calculating with 20 minutes arcs. In order to find out which arc length provides a better solution, an extreme cases were tested. For the month May 2013 10, 15, 20 and 30 minute arcs were introduced with an unrealistic bias degree of 5 (figure V.3).

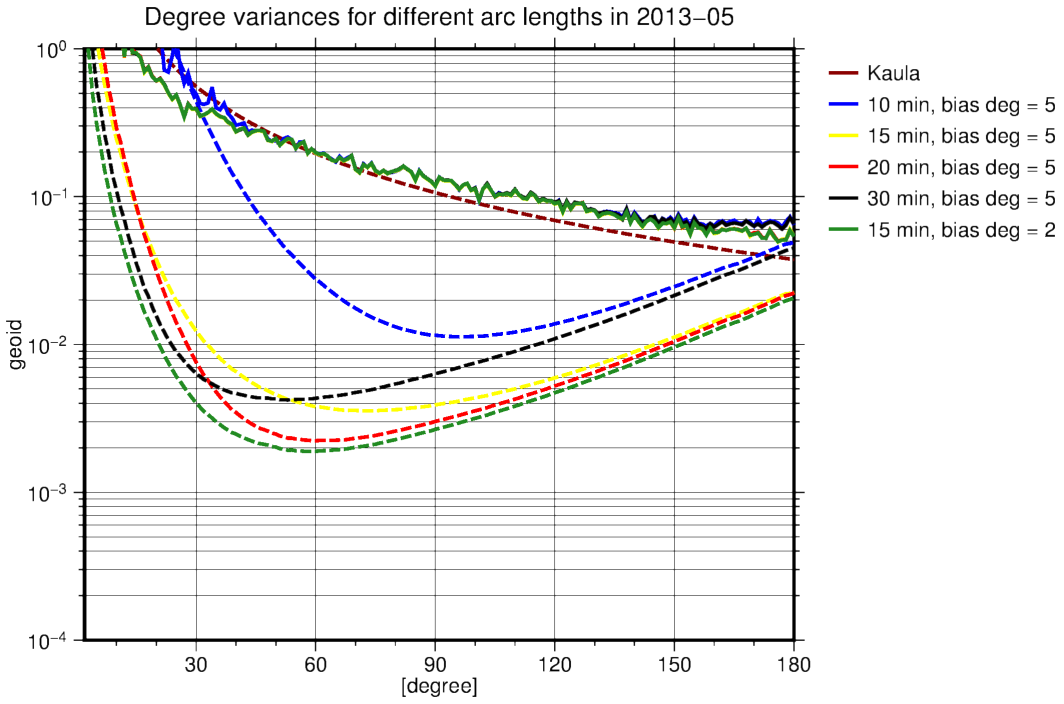

Figure V.3: Degree variances for 2013-5 with a bias degree 5 and different arc lengths

Only the 15 and 20 minute arcs (yellow and red line) were able to produce a realistic result compared to the the bias degree 2 (green line). Still, only in the higher frequencies.
Turning down the bias degree let to the result of degree two and 15 minutes arc length. However, it might be possible to find a better combination, for example by lowering the degree of the Legendre polynomial even more, but this has to be investigated for each month individually.

The computation is executed on a monthly level, thus a global coverage is almost achieved. Two months are a reasonable time span as well, since within 61 days one repeat cycle is completed. Results for one or two months are interchangeable in the RADA, but one month provides easier calculation error handling (e.g. server crashes).
Concluding this chapter, table V.2 lists the settings used for the computation of the static gravity field.

Table V.2: Chosen settings for the gravity field computation with the raw accelerometer data approach

Spherical harmonic expansion	d/o 2 - 250
Estimation	monthly
Arc length	15 minutes
Bias estimation	yes
Degree for Legendre polynomial of bias	2
Estimation of angular accelerations	yes
Estimation of common mode accelerations	yes
Estimation of constant calibration parameters	yes
Estimation of trend calibration parameters	yes
Estimation of the k_2 factor	yes
Estimation of accelerometer positions	yes
Degree for interpolation	4
Degree for numerical integration	5

Part VI

Results

The whole processing of the GOCE data was done within the software package GROOPS[13] developed at the Institute of Geodesy, working group Theoretical Geodesy and Satellite Geodesy at the Graz University of Technology and the University of Bonn. The spherical harmonic series was truncated at degree and order 250, representing a spatial resolution of about 80 km. Nevertheless, recent models go up to d/o 280. The raw accelerometer data approach is suitable for such dimension as well, however, due to calculation time issues, d/o 250 was chosen. The processing took about 600 hours, which is almost one month of computing with 24 cores and 250 GB of RAM. The minor part was the preprocessing, summing up to roughly 150 hours, giving way to just less than 20 days of building the normal equations, where one month of normal equations consumes around 14 GB of memory space, so more than 500 GB for all months. Eventually, eliminating on normal equation level, accumulating the monthly solutions and solving the normal equations took another day.

1 RADA solution and validation

Starting with the solution, the result of the raw accelerometer data approach in terms of geoid heights is shown below (figure VI.1).

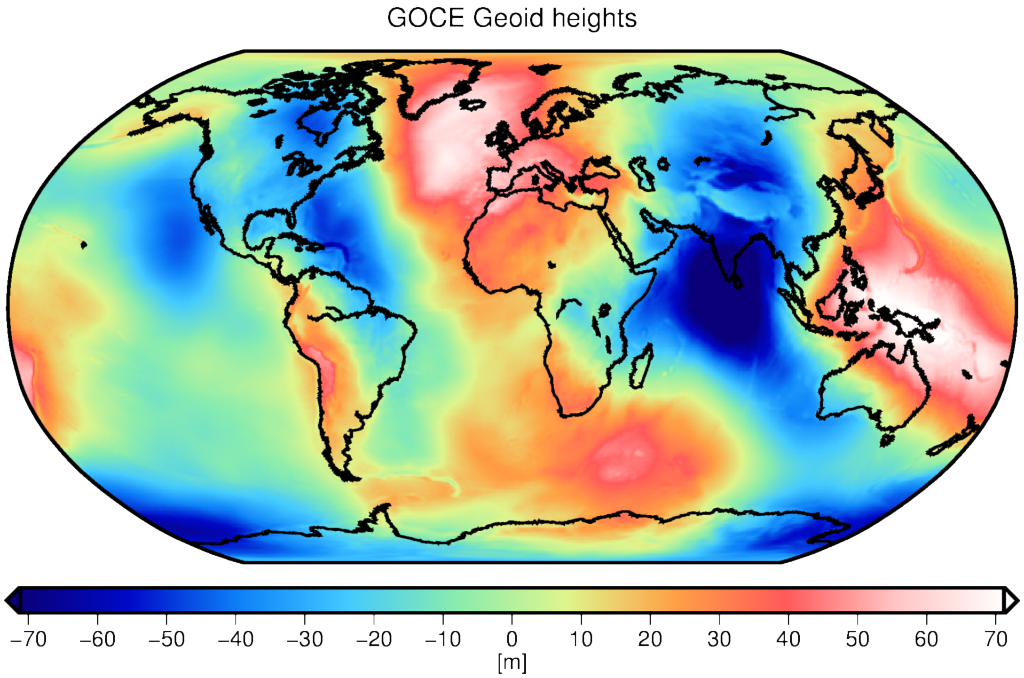

Figure VI.1: Geoid heights GOCE RADA

From a visual point of view, it looks like any other recent geoid solution, therefore a table with the most important statistical facts compared to another GOCE solution, the TIM5 (time-wise approach) computed

[13] Gravity Recovery Object Orientated Programming System

within the HPF, may help (table VI.1). Note that this and the following solutions are regularized. Therefore, the polar gap does not produce such large meaningless values, but still the results of 6° around the poles are random.

Table VI.1: Statistics RADA and TIM5 in terms of geoid heights

	RADA [m]	TIM5 (d/o 250) [m]
Min	−104.758	−106.459
Max	85.861	85.918
RMS	30.071	30.575
Mean	0.002	−0.0001

The minimal value is slightly larger in the RADA than in the TIM5 release, vice versa is the maximum. In the RADA the root mean square error is a bit smaller. The fact that the mean value is close to zero coincides with the expectation value of global geoid heights, which is zero.
For the sake of completeness, the gravity anomalies and the radial gravity gradient are also shown in figure VI.2a and VI.2b. The respective statistical values, compared to the TIM5, can be taken from table VI.2.

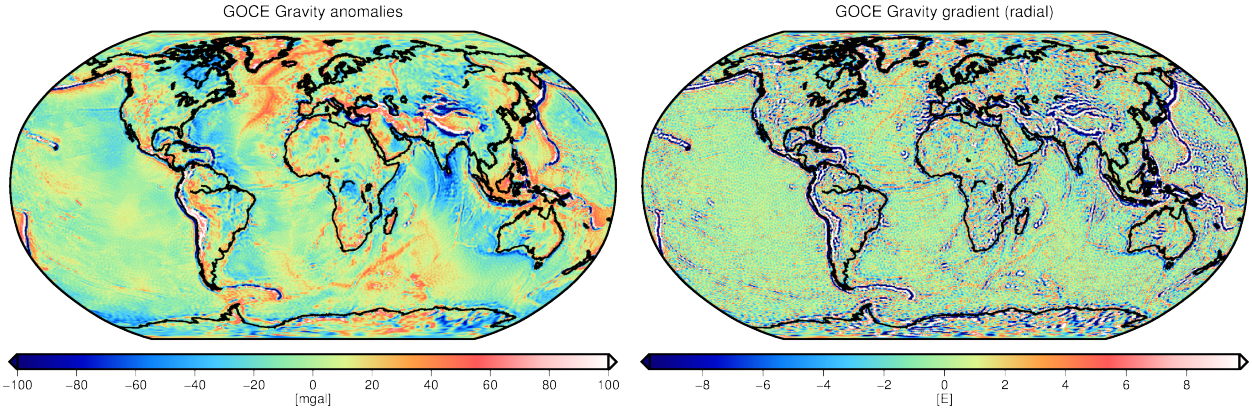

(a) Gravity anomalies (b) Radial gravity gradient

Figure VI.2: GOCE RADA gravity field products

Table VI.2: Statistics RADA and TIM5 in terms of gravity anomalies (left) and the radial gravity gradient (right)

	RADA [mgal]	TIM5 (d/o 250) [mgal]
MIN	−312.301	−309.473
MAX	379.728	374.935
RMS	29.057	28.952
Mean	$2 \cdot 10^{-5}$	$-6 \cdot 10^{-5}$

RADA [E]	TIM5 (d/o 250) [E]
−60.975	−60.951
89.677	87.816
5.471	5.369
$-1 \cdot 10^{-5}$	$-1 \cdot 10^{-6}$

Analysing the RADA solution in the spatial domain and comparing it to other gravity field models are done by subtracting the models on a global level for different degrees. By using the TIM5 as a comparison, the analysis can be divided into two parts: First the difference for the low degrees, where imperfections of the gradiometer become apparent and second the comparison for the high degrees showing noise and some systematic behaviour.
For the low degrees (d/o 2 - 100) the differences in geoid heights to the TIM5 are given in figure VI.3a.

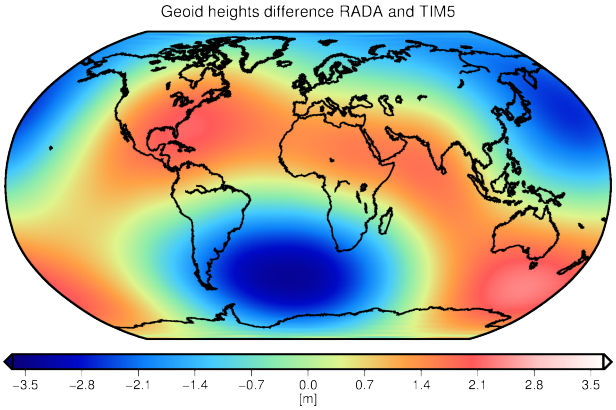

(a) RADA - TIM5

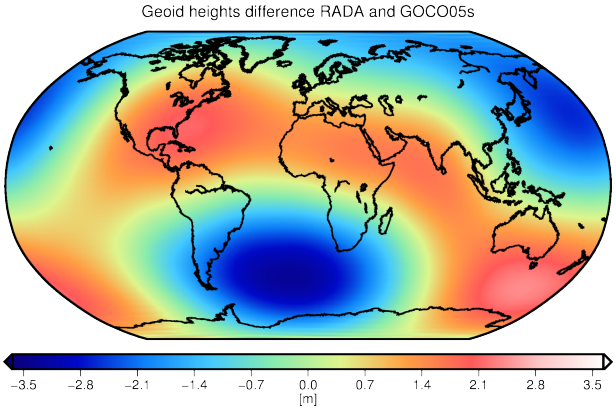

(b) RADA - GOCO05s

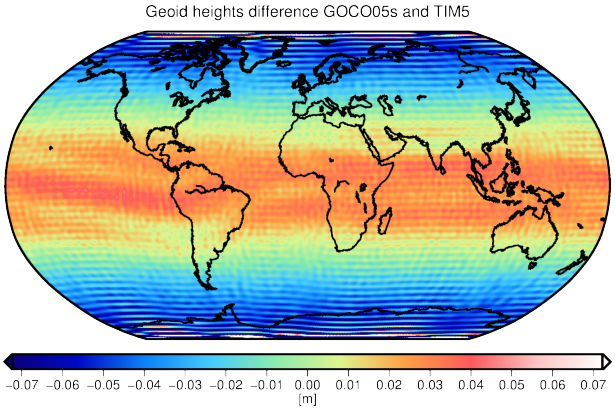

(c) GOCO05s - TIM5

Figure VI.3: Difference in geoid heights for degrees 2 to 100

The systematic offset of about 3 m is obvious. In order to proof that the difference is caused by the RADA, another model, the GOCO05s is added and the two other possible differences are built (figure VI.3b and VI.3c). It can be clearly stated that the difference is caused by the raw accelerometer approach. Mind the different scaling between the images, the right one is almost hundred times smaller in magnitude. The small disparity between the GOCO05s and the TIM5 can be explained with ionospheric disturbances in the SST-hl solution of the TIM5 and the fact that the c_{20} coefficient in the GOCO05s is estimated via SLR solutions. Keep in mind that the RADA model only contains EGG data, which cannot map the low frequencies properly. When adding an SST-hl solution to normal equation level to the raw accelerometer data approach, these differences vanish easily.
For the high degrees (100 to 250), given in gravity anomalies this time (figure VI.4), the difference shows mainly random noise.

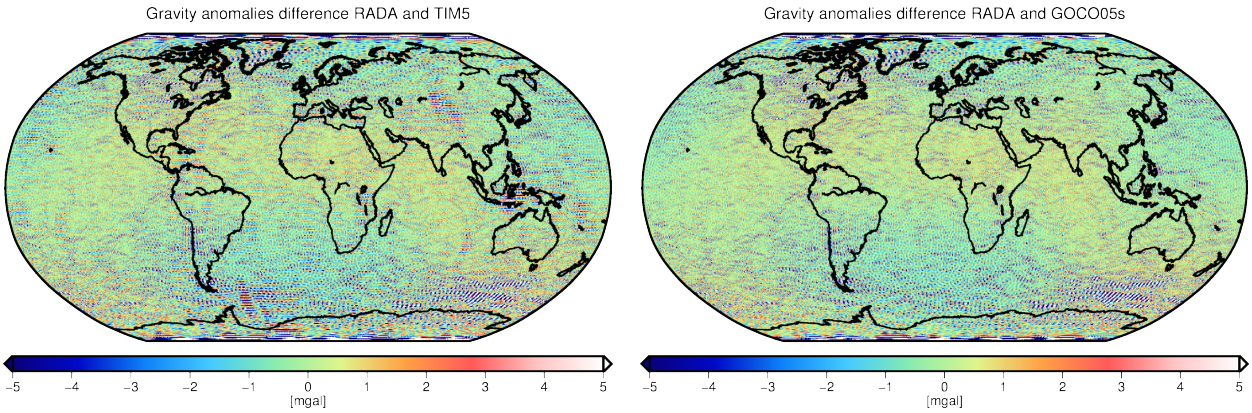

(a) RADA - TIM5 (b) RADA - GOCO05s

Figure VI.4: Differences for the degrees 100 to 250 expressed in gravity anomalies

Only within the TIM5 there seems to be some conspicuous spots north of the Weddell Sea and in central Asia (China - Kazakhstan - Mongolia, figure left). There are no turbulences in these areas in the RADA solution.

When analysing the quality of a gravity field model, the degree variances, the formal error and the differences to other models are an appropriate tool, which indicates the signal and the error at every degree of calculation. Thus, the following comparisons take place in the spectral domain. It has to be noted that the polar gap caused by the orbit inclination of 96° was excluded in the degree variance plots.

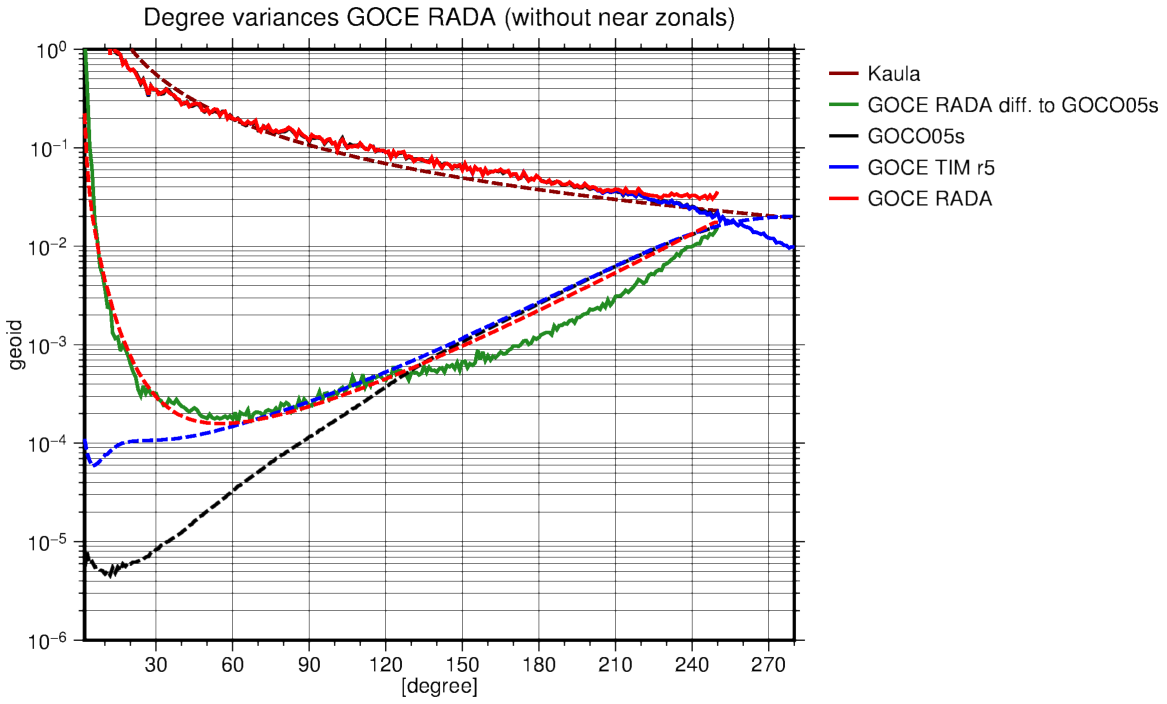

Figure VI.5: Degree variances GOCE RADA non regularized solution

From the degree variances of the RADA model (figure VI.5) it can be seen, that the signal (red) follows

the true gravity field signal. In this case the truth is defined by the other two models. The other models, GOCO05s and GOCE TIM5 were chosen for two reasons: First, the GOCO05s offers one of the most recent satellite-only gravity field solution, combining the data from 15 different satellites, but mainly GRACE and GOCE. It provides an independent solution for the lower degrees. For the higher degrees mainly GOCE data was incorporated, which is the only satellite mission to provide information in this wave lengths. The TIM5 model was used for this incorporation in the GOCO05s, Thus, the differences in the high degrees between the TIM5 and the GOCO05s are close to zero. Hence, the higher degrees of the GOCO05s can be used as a comparison for the RADA solution resembling a GOCE-only solution. The TIM5 was taken into account to enable a comparison to a GOCE-only solution.
The formal error of the RADA solution (red dotted) follows directly the difference between RADA and GOCO05s for the lower degrees. This is a good indicator for the correct weighting in the least squares adjustment via the VCE. Still, from degree 130 onwards, the difference gets smaller than the formal error, a fact that can be ascribed to the data, which is in both cases obtained from the GOCE satellite. The lower degrees of the TIM5 solution provide a better quality due to its calculation method: Since the EGG measures the high frequency components, the TIM5 uses the GPS tracking data via SST-hl for computing the gravity field up to d/o 150 [Brockmann et al. (2014)]. In the RADA only EGG and star tracker data are processed, as a result, a better solution in the low degrees would be possible using GOCE data.

Adding a regularization according to Kaula's rule, presses the signal against the polynomial of degree four found by Kaula in the 1960ies, which describes the signal's behaviour with increasing d/o. This can improve the solution slightly, as the uncontrolled increase of the error is stopped. However, at some point the regularized signal does not follow the true signal, defined by Kaula's rule, any more and decreases against zero. Adding the regularization (figure VI.6) shows that the RADA solution follows the true signal longer than the others (depicted in the zoom), an indicator for the quality of the solution.

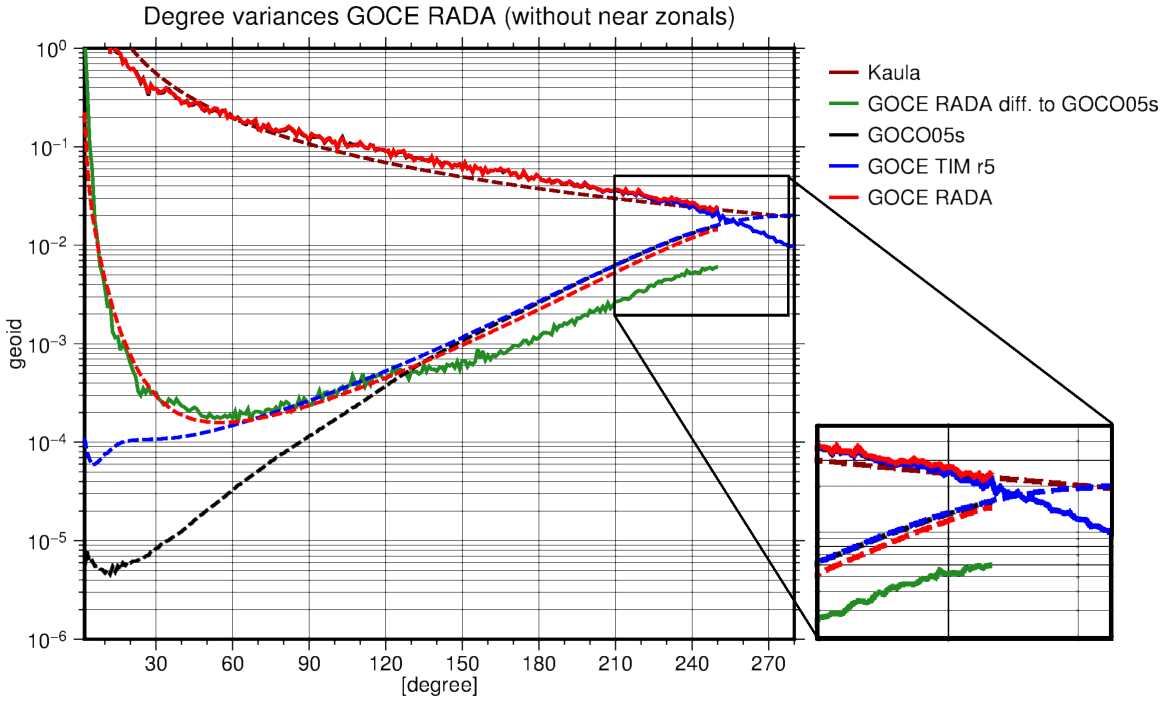

Figure VI.6: Degree variances GOCE RADA regularized solution

Also the formal errors are a slightly lower within the higher degrees. As the processing was only done up to d/o 250, the point of intersection between the signal and the formal error, which defines the point the error exceeds the signal and both cannot be separated any more, is not reached. Thus, the calculation could have been done for a higher degree, roughly estimating the point of intersection for the RADA lies at degree 260.

Another approach of validating the quality of a gravity field solution are the triangles of coefficients, where the standard deviation of each coefficient is plotted. The following figure (fig. VI.7) shows the RADA triangle of coefficients in the regularized (right) and the non-regularized (left) version. For any GOCE solution a inner triangle with high values around the zonal coefficients is striking. This is induced by the polar gap. Regularization (figure right) leads to a significant decrease around the zonal coefficients. The low degree components in the upper part of the triangle show a higher standard deviation due to the EGG resolution in the respective degrees.

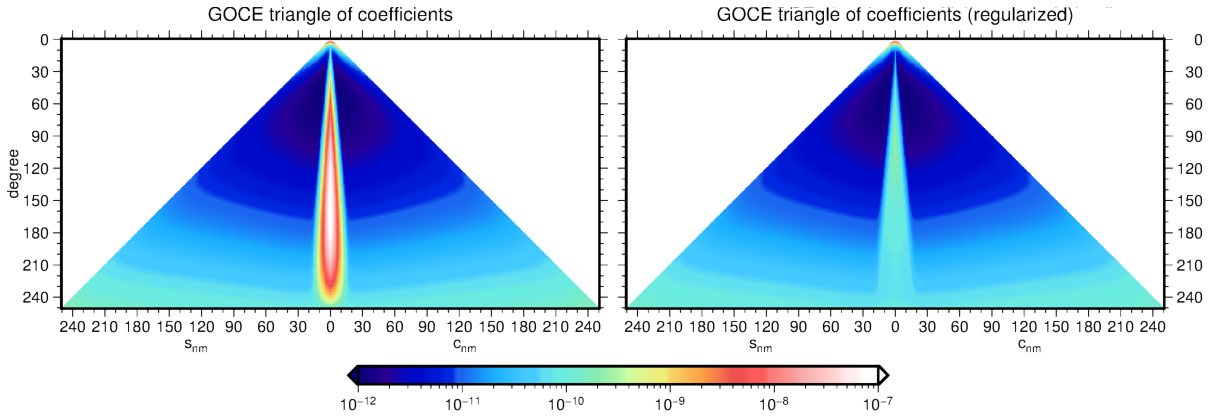

Figure VI.7: Triangle of standard deviation of coefficients non-regularized solution (left) and regularized solution (right)

When treating the impacts of a Kaula regularization, the contribution may help (figure VI.8).

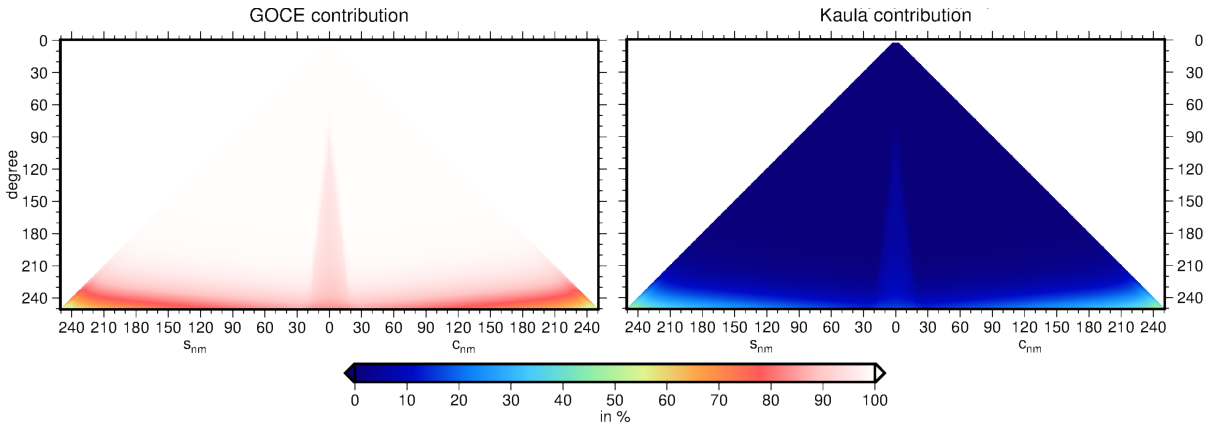

Figure VI.8: Contribution of GOCE data and Kaula regularization to the solution

It shows that the regularizations act more or less only in the zonal area and from degree 210 onwards also in the near sectorial coefficients. Hence, the regularization does not affect the solution too much.

In comparison to the TIM5 release (figure VI.9, right, d/o 250), the impact of regularization on the RADA is smaller (see triangle caused by the polar gap).

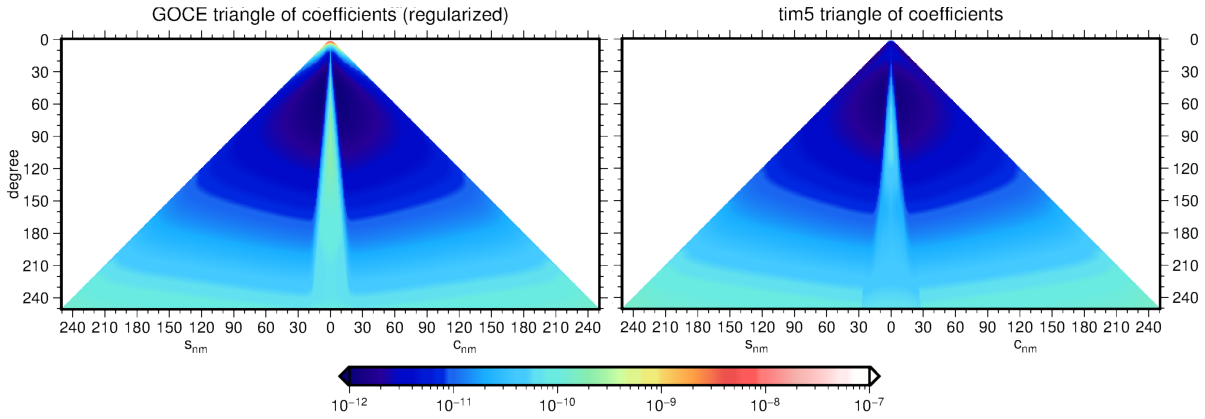

Figure VI.9: Triangle of coefficients: GOCE RADA (left) compared to TIM5 release (right)

Also the formal errors computed with the raw accelerometer data approach are lower in the higher degrees.

2 Independent validation

For a validation independent from GOCE data, only the lower degrees that overlap with static gravity field solutions from GRACE and the high degrees covered within combined satellite/terrestrial model can be taken into account. GOCE is the only data source for the wavelengths in-between. For these the RADA solution provides a lower noise than other up-to-date GOCE models as the TIM5, as seen before in figure VI.6.
The following comparison is based on the ITSG-Grace2014s model, computed by Mayer-Gürr et al. (2014) and the EGM2008 model, the Earth Gravitational Model 2008 from Pavelis et al. (2008), which combines satellite and terrestrial data. Since it was released 2008, GOCE data could not be incorporated.

RADA and ITSG-Grace2014s Validation in the spatial domain shows the same problems of the EGG in the low degrees as before. For any degrees higher than 60 the difference in terms of geoid heights between the ITSG-Grace2014s solution and the RADA gets small, being under 10 cm up to between d/o 60 and d/o 150 (figure VI.10).

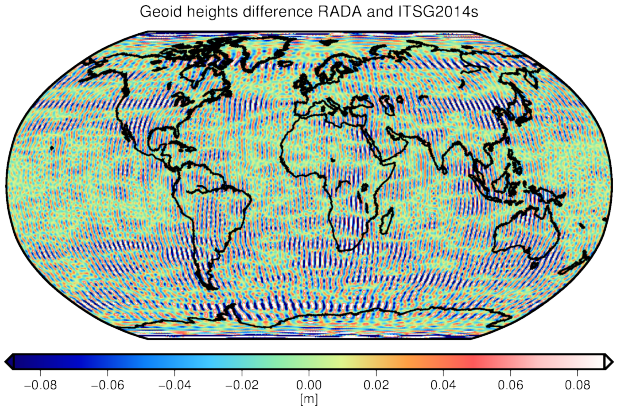

Figure VI.10: Difference RADA - ITSG-Grace2014s in geoid heights for the degrees 60 to 150

Between d/o 60 and 120 the two solutions are as close as possible with differences less than 2 cm. However, the differences show a systematic pattern, which can be ascribed to the GRACE orbit and measurement method. According to the standard deviations derived in the least squares adjustment, the GRACE-only solution is better up to degree 90, then GOCE is in lead. The rise in the difference with increasing degree, may be ascribed to the GRACE model, since the low degrees (60 to 120) are close to each other.

RADA and EGM2008 When comparing to the EGM2008 solution for anything higher than d/o 60 (figure VI.11a), the main visual difference (except of some random noise) is the lack of terrestrial data in some regions (South America, Africa, Antarctica).

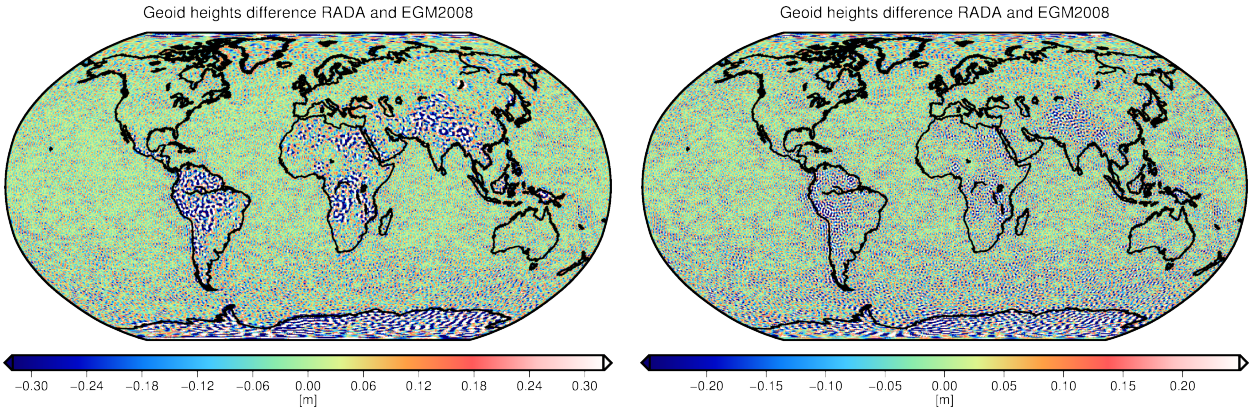

(a) RADA - EGM2008: d/o 60 to 250

(b) RADA - EGM2008: d/o 200 to 250

Figure VI.11: RADA solution in comparison to the EGM2008 model in geoid heights

This affects the EGM2008 model dramatically in the higher degrees. GOCE could observe these wave lengths very well, therefore, these effects do not appear in the RADA solution.
For the degrees 200 to 250, where the EGM2008 has the lower standard deviation, depicted in figure VI.11b, the noise has a higher frequency and systematic errors of the EGM2008 emerge in the radially outwards rolling waves in Africa and South America. The other noise seems to be randomly distributed, thus, a lack of systematic errors in the high degrees of the GOCE RADA solution can be implied.

The validation of the raw accelerometer data approach with the two independent solutions in the spectral domain, as given in the degree variances in figure VI.12, depicts that the RADA and ITSG-Grace2014s solution feature a realistic error behaviour as the formal error curve follows the difference between the solutions quite accurately (green, red and blue line). The RADA model resembles the signal from the EGM2008 closely (black and red). However, the standard deviations of the EGM2008 model seem to be estimated too optimistic, since the difference to the GOCE and the GRACE solution is far away from the line denoting the standard deviation. From d/o 220 onwards the RADA and the EGM2008 get closer to each other. This proofs that in the high degrees, where the EGM2008 model starts to get untouchable because of terrestrial data, both have a good noise estimation. For the degrees in-between the noise estimation of the EGM2008 is not that reliable. There, only other GOCE solutions may be taken into account for a validation, as done before.

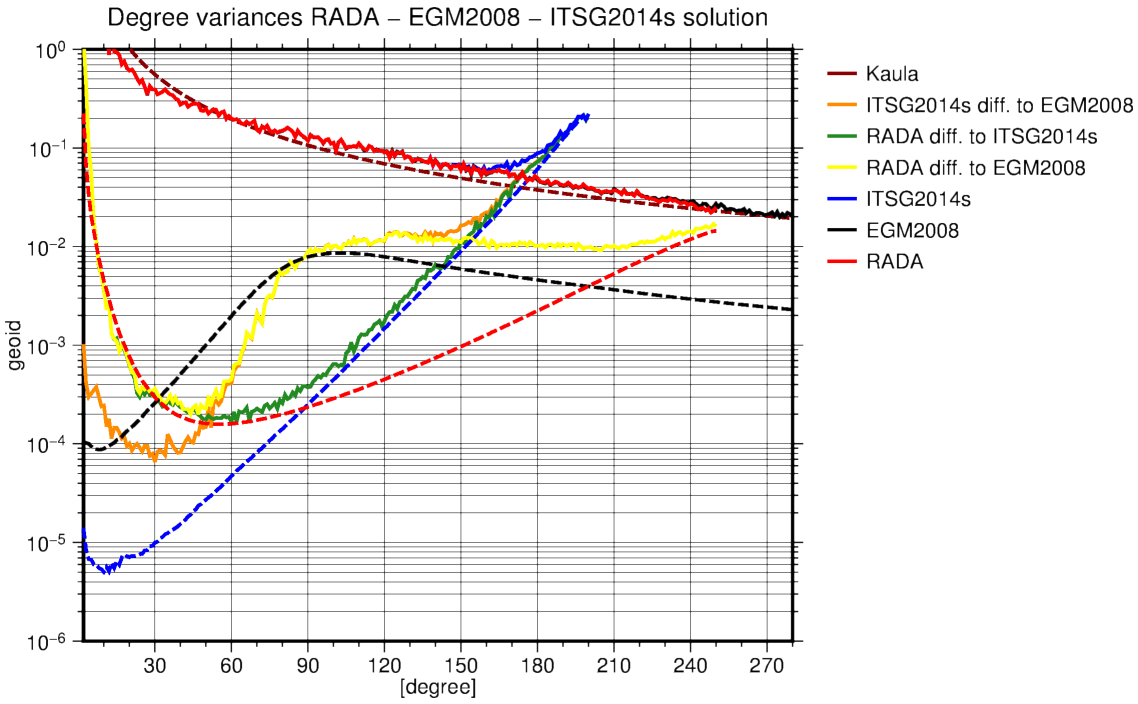

Figure VI.12: Degree variances RADA, ITSG-Grace2014s and EGM2008

Conclusion

Concluding the results, it can be stated that the raw accelerometer data approach for the processing of raw GOCE gradiometer data is not only highly accurate and in some parts even better than recent solutions but also quite flexible in its implementation and open for future developments. In exception the low degrees, where the SST-hl tracking data was not taken into account, the solution provides a highly accurate up-to-date gravity field. For this thesis it was estimated up to degree and order 250, however, an extension of at least 10 or 20 degrees is reasonable. The formal error of the coefficients is plausible and the raw accelerometer data approach provides a realistic solution.

Part VII

Outlook

As the aim of this thesis was to estimate a static gravity field based on raw GOCE accelerometer data, a few notions for future improvements may be given here. Not only deserves the whole GOCE data with its remarkable design further attention but in particular the approach depicted in this thesis. As the whole mission was specifically designed for the HPF processing approach, the proof that a "simple" observations-to-unknown-parameters-linking approach does work well, gives hope to new improvements within GOCE data processing.

Without any further changes to the RADA, the calculation can be drawn to a higher degree, at least 260 or 270. From an analytical point of view, the approach is easy to handle for future improvements, such as adding further parameters in the least squares estimation. Also, the analysis of individual months is simply done. Perhaps the biggest advantage in investigating the data via the raw accelerometer data approach is, that the observations from the accelerometers are treated directly in the least squares adjustment. Therefore, not only the outcome of the linear combinations, the gravity gradients, can be analysed but also the observations themselves. Within the preprocessing step the accelerations can be compared to computed ones from another gravity field, where the estimated corrections are added. Also, a relation between estimated common mode accelerations from the RADA and computed ones via linear combinations may be investigated. Effects that evolve over time, as the worsening of the A2y and A5y axis can be easily revealed in the accelerometer data analysis within the RADA.

The crucial point of the raw accelerometer data approach seems to be the correct estimation and separation of the bias with respect to the common mode accelerations. The described approach of separating them mathematically works well, but still there may be room for further notions. Also the bias' relation to the arc length is a relevant topic for future investigation. Attempts showed that the bias acts very sensitive to the arc length, both increasing and decreasing the 15 minutes. Connected to the arc length, the Legendre polynomial for the bias may not be the best solution, as it seems to oscillate too much if a higher degree than two is used.

Even though the GOCE satellite mission was launched almost a decade ago, lasting for four years, the measured data is neither obsolete nor outdated, on the contrary its unique design facilitates new improvements, be it on the side of instrument processing or of gravity field estimation.

References

Berge, J., Christophe, B., Foulon, B. (2010): GOCE accelerometers data revisited: stability and detector noise

Brockmann, J.-M., Zehentner, N., Höck, E., Pail, R., Loth, I., Mayer-Gürr, T., Schuh, W.-D. (2014): EGM_TIM_RL05: An independent geoid with centimeter accuracy purely based on the GOCE mission.

ESA (2017): Earth Observation Portal (eoPortal) - GOCE satellite mission:
https://directory.eoportal.org/web/eoportal/satellite-missions/g/goce

ESA (2006): GOCE Level 1b Products User Handbook

Fehringer, M., Andre, G., Lamarre, D., Maeusli, D. (2008): GOCE and its Gravity Measurment Systems

Gruber, T., Abrikosov, O., Hugentobler, U. (2014): GOCE Standards, Issue 4

Gruber, T. and Rummel, R. (2014): GOCE Gravity Field Models – Overview and Performance Analysis, 3rd International Gravity Field Service (IGFS) General Assembly, Shanghai, 2014

Mayer-Gürr, T., Pail, R., Gruber, T., Fecher, T., Rexer, M., Schuh, W.-D., Kusche, J., Brockmann, J.-M., Rieser, D., Zehentner, N., Kvas A., Klinger, B., Baur, O., Höck, E., Krauss, S., Jäggi, A. (2015):
The combined satellite gravity field model GOCO05s, Presentation at EGU 2015, Vienna

Mayer-Gürr, T., Zehentner, N., Klinger, B., Kvas, A. (2014): ITSG-Grace2014: a new GRACE gravity field release computed in Graz. - in: GRACE Science Team Meeting (GSTM), 2014

Pavelis, N. K., Holmes, S. A., Kenyon, S. C., Factor, J. K. (2008): An Earth Gravitational Model to Degree 2160: EGM2008, Presentation at EGU 2008, Vienna

Siemes, C. (2017): IMPROVING GOCE L1B GRAVITY GRADIENTS, HPF Reprocessing Workshop, 2/3 February 2017, IAPG

Siemes, C. (2011): GOCE gradiometer calibration and Level 1b data processing, ESA Working Paper EWP-2384

Stummer, C. (2006): Analyse der Gradiometergleichungen der GOCE Satellitenmission zur Schwerefeldbestimmung, Diploma thesis

Stummer, C., Fecher, T., Pail, R. (2011): Alternative method for angular rate determination within the GOCE gradiometer processing

Torge, W., Müller, J. (2012): Geodesy, De Gruyter

Index of abbreviations

Abbreviation	Description
ARF	Accelerometer Reference Frame
CHAMP	Challenging Minisatellite Payload
CoM	Enter of Mass
DFACS	Drag-Free Attitude Control System
d/o	degree and order
EADS	European Aeronautic Defence and Space Company
EFRF	Earth-Fixed Reference Frame
EGG	Electrostatic Gravity Gradiometer
EGM2008	Earth Gravitational Model 2008
ESA	European Space Agency
ESOC	European Space Operations Centre
ESRIN	European Space Research Institute
GFZ	Geoforschungszentrum
GOCE	Gravity field and Steady-state Ocean Circulation Explorer
GPS	Global Positioning System
GRACE	Gravity Recovery And Climate Experiment
GRF	Gradiometer Reference Frame
HPF	High Processing Facility
IRF	Inertial Reference Frame
LSA	Least Squares Adjustment
ONERA	Office National d'études et de Recherches Aérospatiales
PSD	Power Spectral Density
RADA	Raw Accelerometer Data Approach
RFS	Radio Frequency System
SGG	Satellite Gravity Gradiometry
SST-hl	Satellite-to-Satellite Tracking high-low
TIM5	GOCE only model in time-wise approach, release 5
VCE	Variance Component Estimation